

## INFORMATION TO USERS

**This material was produced from a microfilm copy of the original document. While the most advanced technological means to photograph and reproduce this document have been used, the quality is heavily dependent upon the quality of the original submitted.**

**The following explanation of techniques is provided to help you understand markings or patterns which may appear on this reproduction.**

- 1. The sign or "target" for pages apparently lacking from the document photographed is "Missing Page(s)". If it was possible to obtain the missing page(s) or section, they are spliced into the film along with adjacent pages. This may have necessitated cutting thru an image and duplicating adjacent pages to insure you complete continuity.**
- 2. When an image on the film is obliterated with a large round black mark, it is an indication that the photographer suspected that the copy may have moved during exposure and thus cause a blurred image. You will find a good image of the page in the adjacent frame.**
- 3. When a map, drawing or chart, etc., was part of the material being photographed the photographer followed a definite method in "sectioning" the material. It is customary to begin photoing at the upper left hand corner of a large sheet and to continue photoing from left to right in equal sections with a small overlap. If necessary, sectioning is continued again — beginning below the first row and continuing on until complete.**
- 4. The majority of users indicate that the textual content is of greatest value, however, a somewhat higher quality reproduction could be made from "photographs" if essential to the understanding of the dissertation. Silver prints of "photographs" may be ordered at additional charge by writing the Order Department, giving the catalog number, title, author and specific pages you wish reproduced.**
- 5. PLEASE NOTE: Some pages may have indistinct print. Filmed as received.**

**Xerox University Microfilms**

300 North Zeeb Road  
Ann Arbor, Michigan 48106

74-2303

HAN, Kwang Soo, 1931-  
NUCLEAR MAGNETIC RESONANCE IN THE AMORPHOUS  
TRANSITION METAL VZr ALLOY.

The College of William and Mary in  
Virginia, Ph.D., 1973  
Physics, solid state

University Microfilms, A XEROX Company, Ann Arbor, Michigan

NUCLEAR MAGNETIC RESONANCE IN THE  
AMORPHOUS TRANSITION METAL VZr ALLOY

---

A Thesis  
Presented to  
The Faculty of the Department of Physics  
The College of William and Mary in Virginia

---

In Partial Fulfillment  
Of the Requirements for the Degree of  
Doctor of Philosophy

---

by

Kwang Soo Han

August 1973

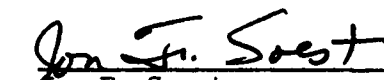
APPROVAL SHEET


This thesis is submitted in partial fulfillment of  
the requirements for the degree of  
Doctor of Philosophy


  
Kwang Soo Han  
Kwang Soo Han

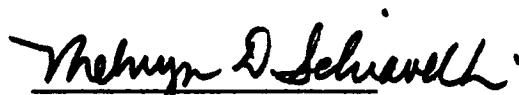
Approved, August 1973

  
Harlan E. Schone  
Harlan E. Schone

  
Jon F. Soest  
Jon F. Soest

  
Roy L. Champion  
Roy L. Champion

  
William J. Kossler  
William J. Kossler

  
Melvyn D. Schiavelli  
Melvyn D. Schiavelli  
Department of Chemistry

NUCLEAR MAGNETIC RESONANCE IN THE  
AMORPHOUS TRANSITION METAL VZr ALLOY

## Table of Contents

	Page
Abstract . . . . .	iii
I. Introduction . . . . .	1
II. Theory and Background. . . . .	4
A. Transition Metal . . . . .	4
B. Knight Shift . . . . .	6
C. Alloys and Local Effects . . . . .	7
D. Quadrupole Effects in VZr Alloy. . . . .	16
E. Behavior of Superconducting Transition Temperature ( $T_c$ ) of Amorphous and Crystalline Metal with respect to Electron Concentration . . . . .	18
III. Experimental Procedure . . . . .	23
A. Preparation of Samples . . . . .	23
B. Target and Substrate . . . . .	25
C. Structure and Composition Analysis of VZr Film . . . . .	25
D. NMR Equipment. . . . .	29
E. General. . . . .	32
IV. Results and Discussion . . . . .	37
A. Knight Shift . . . . .	37
B. Linewidth. . . . .	45
C. Quadrupole Effects . . . . .	54

	Page
V. Acknowledgements . . . . .	59
VI. References . . . . .	60
VII. List of Tables . . . . .	63
VIII. List of Figures. . . . .	64

### Abstract

The nuclear magnetic resonance of  $V^{51}$  in both the amorphous and crystalline phase of VZr alloy film has been investigated in an effort to determine the parameters controlling the electronic structure of the amorphous phase relative to the crystalline phase. Changes in the Knight shift, the line width, and the intensity of the absorption line of  $V^{51}$  for both the amorphous phase and the crystalline phase have been measured at 77°K employing a static magnetic field ranging from 8 to 17 kilogauss.

All observed changes in Knight shift of  $V^{51}$  in the amorphous phase of VZr alloy film are small, and show a slight linear field dependence as compared with that in the corresponding crystalline phase. On the other hand the line width of  $V^{51}$  in the amorphous phase is considerably larger than that in the crystalline phase, and has a strong linear field dependence. This behavior may be accounted for in terms of Friedel oscillations or the rigid band model. The significant decrease in the line intensity of the amorphous phase relative to that of the crystalline appears to be consistent with an all or nothing wipeout model. It is concluded that the quadrupole interaction of  $V^{51}$  with the large electric field gradient, which is

produced by the lattice distortion and redistribution of the occupied electronic states, is probably associated with gas impurities trapped in the amorphous VZr film.

## I. INTRODUCTION

This thesis describes the results of an investigation of the nuclear magnetic resonance (NMR) of  $V^{51}$  in a transition metal VZr alloy which was prepared in a highly disordered state by the RF sputtering process. The purpose of this study is to achieve a better understanding of the changes in nuclear and electronic properties of the transition metal alloy in the amorphous phase as compared with that in the crystalline one.

Vanadium was chosen for the study because it has a large magnetic moment (5.139 nuclear magneton) and a small quadrupole moment, and it forms a solid solution in the amorphous phase with zirconium at room temperature in the RF sputtering process.  $V^{51}$  has a nuclear spin  $I = 7/2$  and a natural abundance of 99.75%. Since  $Zr^{91}$  has a small magnetic moment so that the relative sensitivity of  $Zr^{91}$  magnetic resonance is very small, a  $Zr^{91}$  NMR study was ruled out.

Nuclear magnetic resonance can provide information about the electronic structure of solids as a result of the effect on the nuclei of various interactions with electrons. In metals the most important of such interactions are the magnetic hyperfine interaction between the conduction electrons and the nuclei, and the nuclear quadrupole interaction between nuclei which possess intrinsic

quadrupole moment and the electric field gradient generated by the perturbation of the electronic charge distribution. The measurement of Knight shift, the NMR absorption linewidth, the absorption intensity, and their variation with  $Zr^{91}$  concentration or the applied magnetic field should provide information about the validity of a rigid band model<sup>1</sup>, or the presence of the long range oscillation in the conduction electron density previously noted by Friedel et al<sup>2</sup> in the amorphous and crystalline phases of transition metal alloy.

In the following section of this paper, the theory and background of this problem will be considered. The experimental technique, including a discussion of the factors which affect the accuracy of the measurement, is described in Section III. Section IV presents the experimental results and discussion.

Before proceeding to the next section, it is appropriate to give some idea of what is meant by the term "amorphous metal". A variety of other terms have been used in place of the term amorphous, including: lack of long range order, the presence of only short range order, a completely random distribution of atoms with a statistical spread in interatomic spacing and orientation, or a collection of small ordered units randomly oriented with respect to each other. In many theoretical formulations of amorphous structures the interatomic separation and/or the atomic potential are treated as random variables within certain limits. However, for the present purpose, the best definition of amorphous is that due to the existing experimental limitations. This definition depends on the technique, which might

be X-ray or electron diffraction, or electron microscopy. Field ion microscopy has not yet been employed, as far as the author is aware, although it would seem to be an excellent tool for understanding the amorphous structure. Diffraction patterns for amorphous materials usually exhibit two to four broad halos and give information concerning the average number of nearest neighbors about an atom, and their average separation.

Amorphous materials are prepared under conditions that seek to kinetically prevent the formation of the thermodynamically stable crystalline structure. All preparation techniques accomplish this by restricting the ability of the atom to diffuse; the most common of these being some form of rapid temperature quenching from a state of higher entropy i.e., a liquid or gas phase. Another technique, which often occurs inadvertently, is the introduction of impurities, especially gases. The presence of the other metals can also significantly hinder diffusion and is indicated by a higher temperature required to produce the amorphous to crystalline transformation. In this study the amorphous structures were prepared by sputtering vanadium and zirconium simultaneously onto a water-cooled substrate under an argon plasma.

## II. Theory and Background

### A. Transition Metal

Transition metals are characterized by partially filled d-bands which are usually quite narrow and therefore have a high density of states at the Fermi level. The d-bands usually overlap with a much wider s-band and the d-electrons are more localized than the free electrons. The simplest model of transition metals assume that the s- and d-bands are distinguishable at the Fermi level. The variation with energy of the density of states of an s-band is much slower than that of a narrow d-band, and it has been common practice to assume that the number of electrons in the s-band is in the range of 0.2-1 per atom<sup>3</sup>.

The contribution of the s-band to the total hyperfine interaction can be estimated by means of the free electron energy density of states now. In most cases, however, this is a dangerous approximation because the crystal potential may overlap. Since the s-d mixing is significant, it is useful to characterize the state at the Fermi level by the average fractional s and d character. Consequently, one may define a fractional s and d density of states such that

$$N(E_F) = N_s(E_F) + N_d(E_F) \quad (1)$$

The ratio  $N_s(E_F) / N_d(E_F)$  will depend, in general, on the details of the band structure. If spin-orbit interactions are not too important, then the total magnetic susceptibility of a transition metal can be partitioned into spin and orbital contributions:

$$\chi = \chi_s + \chi_d + \chi_{vv} + \chi_L + \chi_{dia}. \quad (2)$$

The first two terms in Eq. (2) are s and d spin susceptibilities, respectively, which can be related by,

$$\chi = \sum_k \chi_k = \frac{1}{2} (\gamma_e \hbar)^2 N(E_F). \quad (3)$$

$\chi_{vv}$  is a field induced orbital paramagnetic susceptibility which arises from the orbital degeneracy of the atomic d states.  $\chi_{vv}$  is analogous to the temperature independent Van Vleck susceptibility in the magnetic insulators.

$$\chi_{vv} = \frac{1}{4} (\gamma_e \hbar)^2 \sum_k \sum_{k'} \frac{(f_{k'} - f_k)}{E_{k'} - E_k} |\langle k' | L | k \rangle|^2, \quad (4)$$

$$\chi_L = -\frac{1}{2} (\gamma_e \hbar)^2 N(E_F) (m^2 / 3m^2), \quad (5)$$

(Landau diamagnetic susceptibility), and

$$\chi_{dia} = -\frac{e^2}{6mc^2} \sum_i \langle r_i^2 \rangle \quad (6)$$

due to the ion core.

Because of the high density of d states at the Fermi level, the paramagnetic contributions to  $\chi$  in transition metals are much larger than  $\chi_L + \chi_{dia}$ . This is in contrast to the situation in simple metals where

the diamagnetic term usually dominates. In practice, the individual contributions to  $\chi$  cannot be calculated from first principles because of insufficient knowledge about the conduction electron states. One of the important applications of NMR in the transition metals involves the separation of  $\chi$  into its various parts on the basis of the measured resonance shift and relaxation time.

#### B. Knight Shift

When the NMR frequency in a metallic sample is observed, it is found that this frequency differs from that detected from the same nuclear species in a diamagnetic compound, both measurements having been performed in the same static magnetic field. This displacement of NMR frequency in metals is called the Knight shift, after its discoverer, W. D. Knight<sup>4</sup>. Since this shift is generally an order of magnitude or more greater than chemical shifts, it was realized that such a shift is associated with the conduction electrons of the metal.

The Knight shift has been successfully explained in terms of the hyperfine interaction between the nucleus and the non-localized conduction electrons. The important contributions to the total Knight shift in the transition metal are associated with the three paramagnetic contributions to the magnetic susceptibility. The hyperfine Hamiltonian may be written as

$$H = \gamma_n \gamma_e \hbar^2 \mathbf{I} \cdot \Theta, \quad (7)$$

where  $\Theta$  operates on the one-electron spin (S) and orbital angular momentum ( $l$ ) coordinates. Using an obvious notation,

$$\theta = \theta_s + \theta_d + \theta_{orb}, \quad (8)$$

where  $\theta_s = \frac{2}{\hbar} H_{hfs}^{(s)} S_s,$

$$\theta_d = \frac{2}{\hbar} H_{hfs}^{(d)} S_d, \text{ and}$$

$$\theta_{orb} = \left\langle \frac{1}{r^3} \right\rangle l = \frac{1}{\hbar} H_{hfs}^{orb} l.$$

The Knight shift therefore becomes

$$K = K_s + K_d + K_{orb} + \text{higher term,}$$

$$= -\frac{2}{\hbar} [H_{hfs}^{(s)} \chi_s + H_{hfs}^{(d)} \chi_d + H_{hfs}^{orb} \chi_{vv}] + \text{higher order term,}$$

or

$$= a_s \chi_s + a_d \chi_d + a_{orb} \chi_{vv}, \quad (9)$$

where  $H_{hfs}^{(s)}$  and  $H_{hfs}^{(d)}$  are the effective s contact and d-spin (core polarization) hyperfine field per electron respectively, and  $H_{hfs}^{(orb)}$  is the orbital hyperfine field per unit orbital angular momentum. Since  $H_{hfs}^{(d)}$  is negative while  $H_{hfs}^{(s)}$  and  $H_{hfs}^{orb}$  are positive, the total shift in transition metals may be of either sign. For instance, the orbital term dominates in  $V^5$ , VCr alloy<sup>6</sup>,  $W^7$ , and  $Nb^8$ . According to Butterworth and Drain<sup>6</sup>, about 2% of the total paramagnetism of pure vanadium is due to 4s spin paramagnetism. About 50% is orbital paramagnetism and the remainder is due to 3d spin paramagnetism. This is not surprising since these metals have roughly half-filled d-bands, encouraging orbital effects, whereas Pt, Pd and Rh have almost filled d-bands so that d-core polarization effects will dominate.

### C. Alloys and Local Effects

The introduction of a foreign atom in a pure metal has two main effects: (1) the NMR line broadens, (2) there is usually a shift

in the resonance frequency for a given external magnetic field. The change in Knight shift,  $\Delta K$ , results from oscillatory variations in the conduction electron charge density about the solute ions. That is to say, any impurity in a metal will produce a charge disturbance. Atomic size and electronegativity effects cause this to be true, to a limited extent even in the case when the valence of the host and that of the solute are identical. The conduction electrons act to screen the

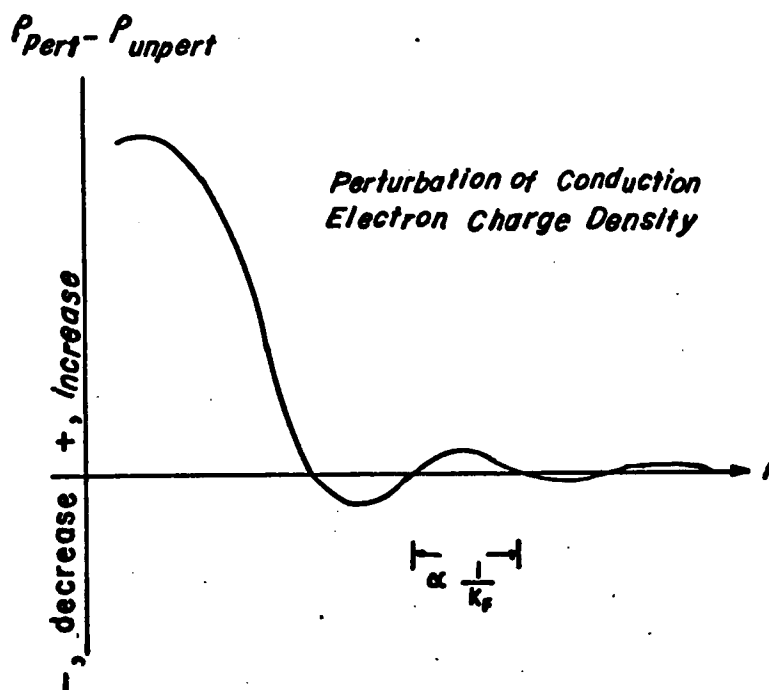


Figure 1. Schematic illustration of conduction electron charge screening induced in a metal host by a single impurity at  $r=0$ . The half-period of the Friedel oscillations, which is proportional to  $1/k_F$  is indicated.

charge difference associated with the impurity. There will be a build up or decrease in the total conduction electron charge in the vicinity of the impurity depending on the sign of the sum of charge terms. The perturbation of conduction electron charge density is illustrated in Figure 1. There is a highly local "main peak" with the familiar Friedel oscillations to the outside. These arise from the presence of a conduction electron Fermi surface and have a period which is inversely proportional to  $2k_F$ , i.e., the extremal caliper of the Fermi surface in the direction in question.

The line broadening is a consequence of the same charge redistribution phenomenon. Since the impurity ions are randomly distributed, solvent nuclei at different distances from the impurity will suffer different shifts in their resonance frequencies. When summed over all the solvent nuclei, this produces line broadening. This phenomenon is similar in some respect to the broadening caused by the anisotropic Knight shift. It should be noted that the line broadening due to alloying will be field dependent. Another possible source of line broadening in this study of the VZr alloy in both the amorphous and crystalline state will be the anisotropic Knight shift broadening and second order quadrupole broadening. With the explicit assumptions that only inhomogeneous Knight shift broadening is present, Blandin and Daniel<sup>2</sup> derived the rule that the line width should increase proportionally to the square root of the concentration in the infinitely dilute alloy. Therefore, it is not expected that such a concentration dependence will be observed in the highly disordered VZr alloy studied here. Indeed the data on the alloys of silver and copper analyzed by Blandin and Daniel show only a feeble agreement with this square root rule.

In order to assess the adequacy of the Blandin and Daniel theory for the VZr alloy investigated here, it will be useful to discuss their theory and the assumptions entering into it. They consider only the case of heterovalent alloys. Electrical neutrality requires a redistribution of the conduction electrons so as to produce a screening of the perturbing potential which is spherically symmetric and limited in range to the atomic sphere of the impurity ion. Explicitly assuming a free electron model and Bloch functions, they use standard scattering theory in order to calculate an expression for  $\Delta\rho(r)$ , the change in the electrical charge density introduced by the shielded impurity potential, in terms of phase shifts in the free electron wavefunctions. Assuming the proportionality of the Knight shift to the electric charge density at the nucleus, they obtain the simple expression

$$\frac{\Delta K_j}{K} = \frac{\Delta\rho(\vec{R}_j)}{\rho},$$

where  $\Delta K_j$  is the change of Knight shift experienced by the nucleus at  $R_j$ . To represent the impurity potential they choose a spherical well with the same radius as the solute ion and a depth sufficient to attract the electronic charge required for the screening. They invoke the Friedel sum rule connecting the phase shifts with the impurity charge and use Blatt's phase shift<sup>9</sup>, which accommodates any size effects by means of an effective charge, to calculate a spectrum of Knight shifts for silver in alloys of AgCd, AgIn and AgSn. Finally to obtain an expression for the average Knight shift of the solvent nuclei in low concentration heterovalent alloys, they further assume a random substitutional alloy, that electrons on the Fermi surface undergo no

multiple scattering from the dissolved impurities, and that the net excess electron density is due to the isolated impurities whence

$$\frac{\Delta K}{K} = C \sum \alpha_l \sin^2 \eta_l + \beta_l \sin 2\eta_l, \quad (10)$$

where C is the concentration,  $\eta$  are phase shifts. The  $\alpha_l$  and  $\beta_l$  are given by the following combinations of spherical Bessel and Neumann functions:

$$\alpha_l = (2l+1) \sum_R [n_l^2(kR) + j_l^2(kR)],$$

and

$$\beta_l = -(2l+1) \sum_R j_l(kR) n_l(kR).$$

The only other assumption entering into their prediction for line broadening is that the contribution due to the impurity is much greater than the line width characteristic of the pure solvent.

The following observations are offered concerning the applicability of the theory of Blandin and Daniel<sup>2</sup> outlined above to the data obtained in the study of the amorphous VZr alloy. If we consider the amorphous phase to be liquid-like, then the small decrease of Knight shift observed in the amorphous phase VZr alloy would seem to imply that it is free electron like, similar to most metals.

Ziman<sup>10</sup> argued that small change observed in Knight shift for most metals indicates that a free electron picture of metals is more nearly correct than was previously recognized. Furthermore the phase shift description of Blandin and Daniel's theory used by Odle and Flynn<sup>11</sup> using the newly derived phase shifts have been partially successful in describing Knight shift versus concentration behavior in liquid

alloys. Thus it might be expected that the Blandin-Daniel theory will be pertinent for amorphous VZr alloys, as it is for silver or copper alloys, to which it was originally applied.

The assumptions in their theory of a spherical Fermi surface (purely s-character for the electronic wave functions) and effective mass identical to the normal electron mass, would however appear to be suspect in view of the band structure calculations and Fermi surface of vanadium<sup>12,13</sup>.

The Blandin-Daniel theory<sup>2</sup> includes only changes in the electron density. No consideration is given to possible changes in the magnetic susceptibility produced by alloying. This is certainly questionable, since the Knight shift is known to depend on the electronic susceptibility. Although changes in susceptibility could be incorporated into a refined version of the scattering theory through changes induced in the density of states at the Fermi surface by phase shifts, such a refinement has not yet been attempted, probably because comparisons between theory and experiment have so far been only semi-quantitative at best.

A conceptual scheme which is frequently employed in considering the properties of alloys is the so-called rigid band model<sup>1</sup> discussed in the earlier section. For a pure metal the electronic structure may be fairly well accounted for on the basis of the present theory. Employing single particle Bloch functions, the energy structure of the pure metal is adequately described in terms of Brillouin zones,

energy gaps, energy bands, a Fermi surface, density of states<sup>1</sup> etc. The simplest form of the rigid band model of alloys assumes that the constant energy surfaces and density of states characteristic of the solvent are not modified by alloying. The consequences of adding the solute are adding or subtracting electrons from the band, depending on the relative valence of the solute. Thus the Fermi surface will be either dilated or contracted by adding the solute. For example if we consider 3d transition metal alloy of Ti-V and V-Cr system, there is a gradual increase in  $K$  with electron to atom ratio, with a peak at about 5.6 electron to atom ( $e/a$ ). Between  $e/a = 5.6$  to 6, there is a gradual decrease in  $K$ . These are shown in Figure 2.

The complex nature of Knight shift sometimes causes the correlation of Knight shift, susceptibility, and specific heat to be obscured, and the fact that  $K$  does not follow the density of states curve is not necessarily an indication of non-rigid band behavior. To give a further picture of the shape of the density of states curve for 3d and 4d transition metal alloy mentioned above, we show the total susceptibility and density of states data in Figure 3. Both for the 3d and 4d series, there is a possible cusp at  $e/a = 5$ . Both susceptibility  $\chi$  curves have quite similar behavior. From this picture we get a different impression of the density of states curve than from the curve obtained from specific heat ( $\gamma$ ) data as shown in Figure 3. Thus there is discrepancy between the  $\gamma$  curve on one hand, and the  $\chi$  curve on the other. Depending on which curves are used, the Knight shift data may be interpreted in a quite different manner. In either case there

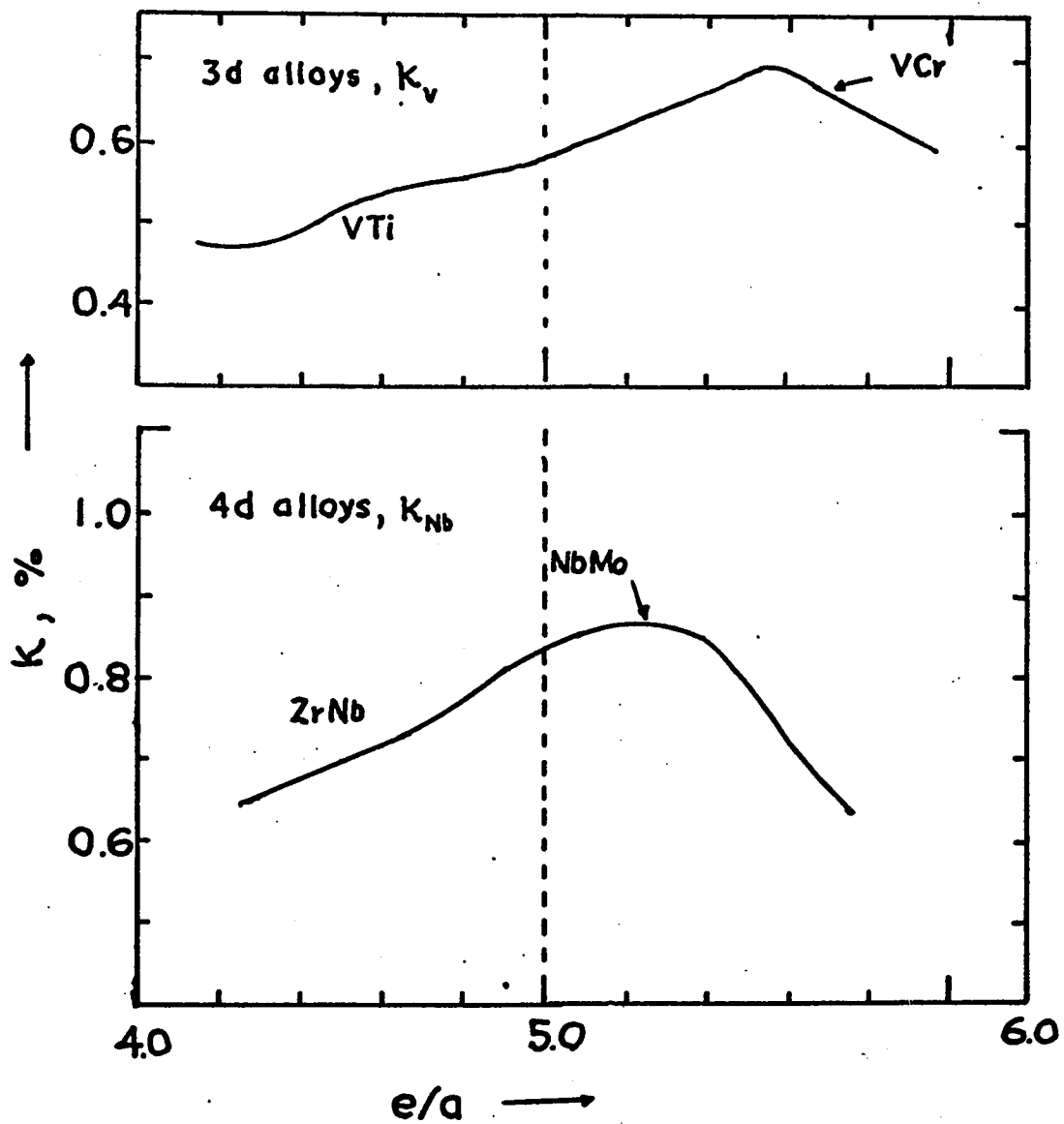
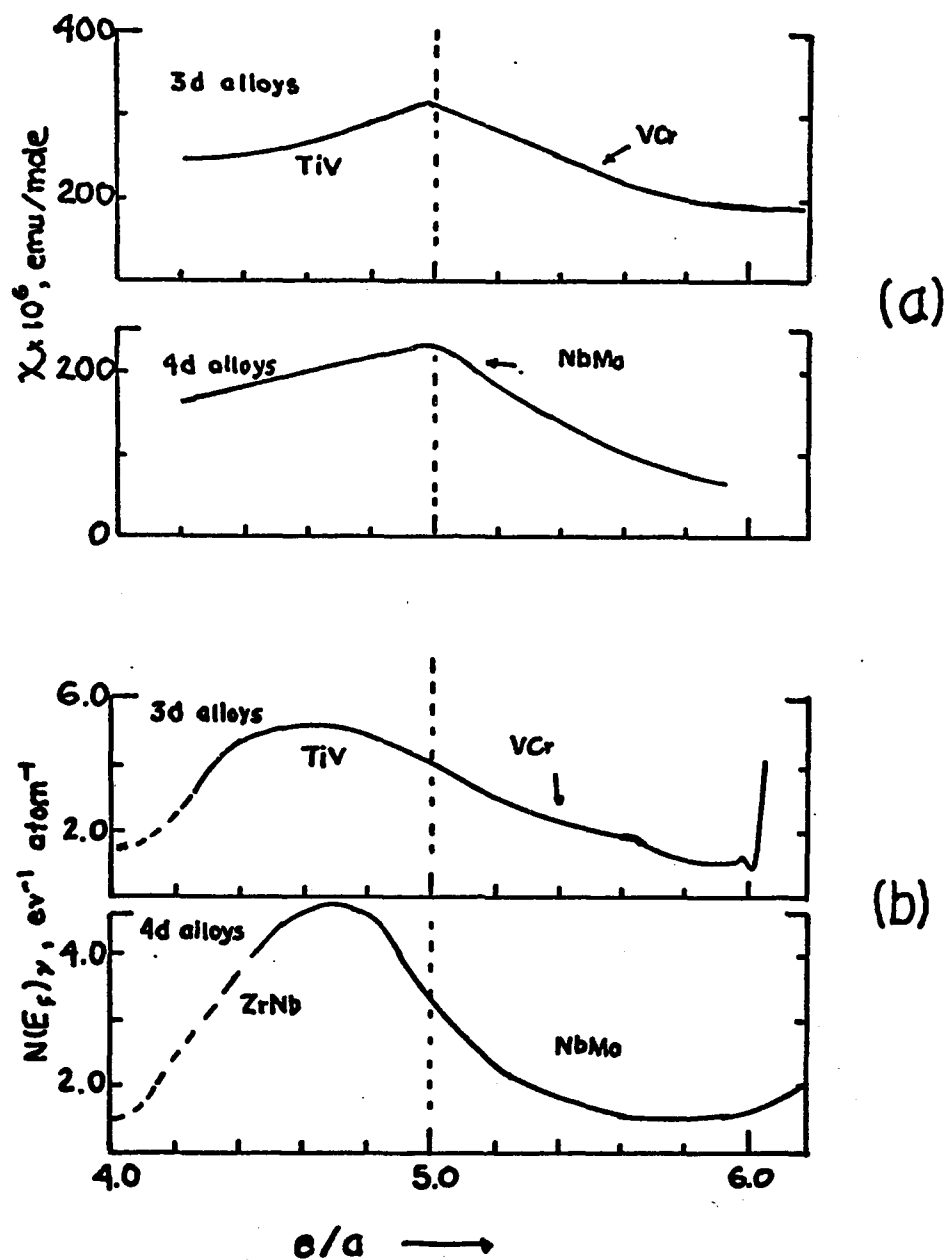


Figure 2. Variation of Knight shift with  $e/a$  ratio for b.c.c. transition metals of the 3d and 4d rows. The data were taken from the following sources: Ti-V (18), V-Cr (18, 19), Zr-Nb, Nb-Mo (15)



**Figure 3.** Variation of (a) susceptibility and (b) density of states as measured by electronic specific heat, with  $e/a$  ratio for b.c.c. transition metals of 3d and 4d rows. The data were taken from the following sources: Ti-V (18), V-Cr (18, 19), Zr-Nb (15), Nb-Mo (14).

is no direct correlation between  $K$  and the other data and there must be an interplay of several terms as a function of  $e/a$ . A number of attempts have been made using  $\gamma$ ,  $\chi$ ,  $\kappa$  as well as  $T_1$  data and the Korringa relation to derive the various contributions to  $K$ . For example the results of Figure 2 and 3 have been explained (Ref. 6, 14, 15) by a two-band model for the Pauli term as in Eq. 9, with estimates of the Van Vleck orbital effects. Although these do explain the results, the description is not unique. An alternative explanation in terms of varying s-d mixture in a single band has been offered (Ref. 16, 17) to explain the maximum in  $K$  at  $e/a \sim 5.6$ . In the region above  $e/a = 5.6$ , both the specific heat  $\gamma$  and susceptibility  $\chi$  are decreasing. Within this model, the decrease in  $K$  arises from a Pauli contribution which becomes less negative, and in fact, positive with increasing  $e/a$ . Only 10 to 15 percent s-character in the d-band is required to balance or overtake the negative d-core polarization terms. Changes in s-character of only a few percent can produce the observed variation in  $K$ . If the hybridization model is proven valid, the Knight shift can provide a useful probe of the variation of the density of s states in "d" bands.

#### D. Quadrupole Effects in VZr Alloy

It was observed that the impurities were necessary to stabilize an "amorphous" structure in the sputtered VZr alloy films. Thus oxygen and other residual gas molecules trapped in VZr alloy film may play an important role in the intensity and width of NMR lines in the amorphous VZr films. For instance the intensity of NMR line, which is defined to

be the product of the peak to peak height and width, is about five times smaller than the intensity of the NMR line after annealing to 900°C. Therefore it is worthwhile discussing quadrupole effects due to the formation of the amorphous state.

The experiments of Bloembergen and Rowland<sup>18</sup> have shown that the intensity of the nuclear resonance signal in metallic copper decreases rapidly when the copper is cold worked or small quantities of the other elements are alloyed with it. These results require that each solute atom produces a substantial field gradient which acts on the copper nuclear quadrupole moments of as many as 85 neighboring nuclei. Kohn and Vosko<sup>19</sup> showed that field gradients, of approximately the required magnitude, arise from the redistribution of the conduction electron charge near the solute atoms. At large distances from a solute atom the electron density behaves as  $\cos(2k_0 r + \varphi) / r^3$ , where  $k_0$  is the Fermi wave number and  $\varphi$  is a phase angle. Such an oscillatory behavior is a consequence of a discontinuous drop at the Fermi surface of  $n(k)$ , the occupation probability of the conduction band state with wave vector  $k$ . According to Kohn and Vosko's calculation, the electric field gradient  $q$  at the  $n^{\text{th}}$  site is given by

$$q = \alpha \frac{2\pi A \cos(2k_0 r + \varphi)}{r^3},$$

where  $\alpha$  is an enhancement factor which measure the increase of  $q$  over its value in a plane wave theory without antishielding.  $A$  and  $\varphi$  are determined by the phase shifts  $\eta_l$  in the following expressions:

$$A = \frac{1}{2\pi^2} \left( \left\{ \sum_l (2l+1) [-\sin \eta_l \cos(\eta_l - l\pi)]^2 + \left\{ \sum_l (2l+1) [-\sin \eta_l \sin(\eta_l - l\pi)]^2 \right\}^{\frac{1}{2}} \right\}^{\frac{1}{2}} \right),$$

$$\text{and } \varphi = \tan^{-1} \frac{\sum_{\ell} (2\ell+1) \cos(\eta_{\ell} - \ell\pi)}{\sum_{\ell} (2\ell+1) \sin \eta_{\ell} \sin(\eta_{\ell} - \ell\pi)} .$$

Rowland<sup>20</sup> has used their  $q$  value for various different solutes and obtained the number of affected copper nuclei  $n$  and the corresponding value of  $q_0$  in the following concentration dependence of the intensity.

$$I = I_0 (1 - C)^n ,$$

where  $C$  is the atomic concentration of solute and  $n$  is the number of copper nuclei affected. Thus Kohn and Vosko's theory is in agreement with Rowland's result.

Recently Meerwall and Rowland<sup>21</sup> investigated  $V^{51}$  quadrupole effects in vanadium transition metal alloys. Their results show these effects to be several times smaller for transition metal (substitutional) solutes than for interstitial oxygen and nitrogen in vanadium. The solute dependence suggests that field gradients around substitutional atoms arise mainly in response to local lattice distortion rather than the shielding of the excess charge of the solute. They estimated that the all-or-nothing wipeout model<sup>21</sup>, when applied to the interstitial alloys, yields wipeout numbers  $n_1 = 126 \pm 7$  for nitrogen in V and  $n = 194 \pm 12$  for oxygen in V. This model assumes that the contribution to the NMR line is lost for nuclei inside a sphere centered on the defect.

#### E. Behavior of Superconducting Transition Temperature ( $T_c$ ) of

##### Amorphous and Crystalline Metal with Respect to Electron Concentration

It is worthwhile here to mention the variation of  $T_c$  of amorphous and crystalline metals with respect to electron concentration measured by Collver and Hammond<sup>22</sup>, because it may be correlated to the variation of Knight shift of the amorphous transition metal alloys

with respect to electron concentration. They showed that  $T_c$  of the amorphous film of the 4d and 5d transition metal alloys increases as a function of the number of electrons per atom in a smooth nearly linear fashion to a definite triangular peak near the middle of the d series. The peak occurs for the 4d series at  $e/a \sim 6.4$  in contrast to the crystalline maximum at 6.7. The  $T_c$  decreases at nearly the same slope, followed by a more rapid decrease at  $e/a \sim 7.0$ . This is shown in Figure 4. The smooth behavior in  $T_c$  across two phase regions of the alloy system demonstrates that  $e/a$  determines  $T_c$  in the "amorphous" state, independent of the normal crystal structure. According to B. C. S. theory<sup>23</sup>,  $T_c$  is related to many normal state properties including electronic density of states and phonon spectrum as follows:

$$T_c \sim \omega_c \exp - \frac{1}{N(E_F) V_{att}}$$

where  $\omega_c$  is the mean phonon frequency,  $N(E_F)$  is the density of states at the Fermi surface, and  $V_{att}$  is the average attractive interaction between electron pairs. In the crystalline state  $N(E_F)$  exhibits a still unexplained correlation with  $1/\theta_D^2$  (and therefore  $1/\langle \omega \rangle$ ), and it is believed to be the factor controlling the electron phonon interaction parameter and  $T_c$ <sup>24,25</sup>. In the amorphous state the  $N(E_F)$  is assumed to be smoothed out versus  $e/a$  by the disorder,<sup>26,27</sup> allowing the variation with  $e/a$  of the amorphous  $T_c$  to be determined by the interaction parameter or other atomic like parameters. In a highly disordered state all structure in  $N(E_F)$  is smeared out, reducing

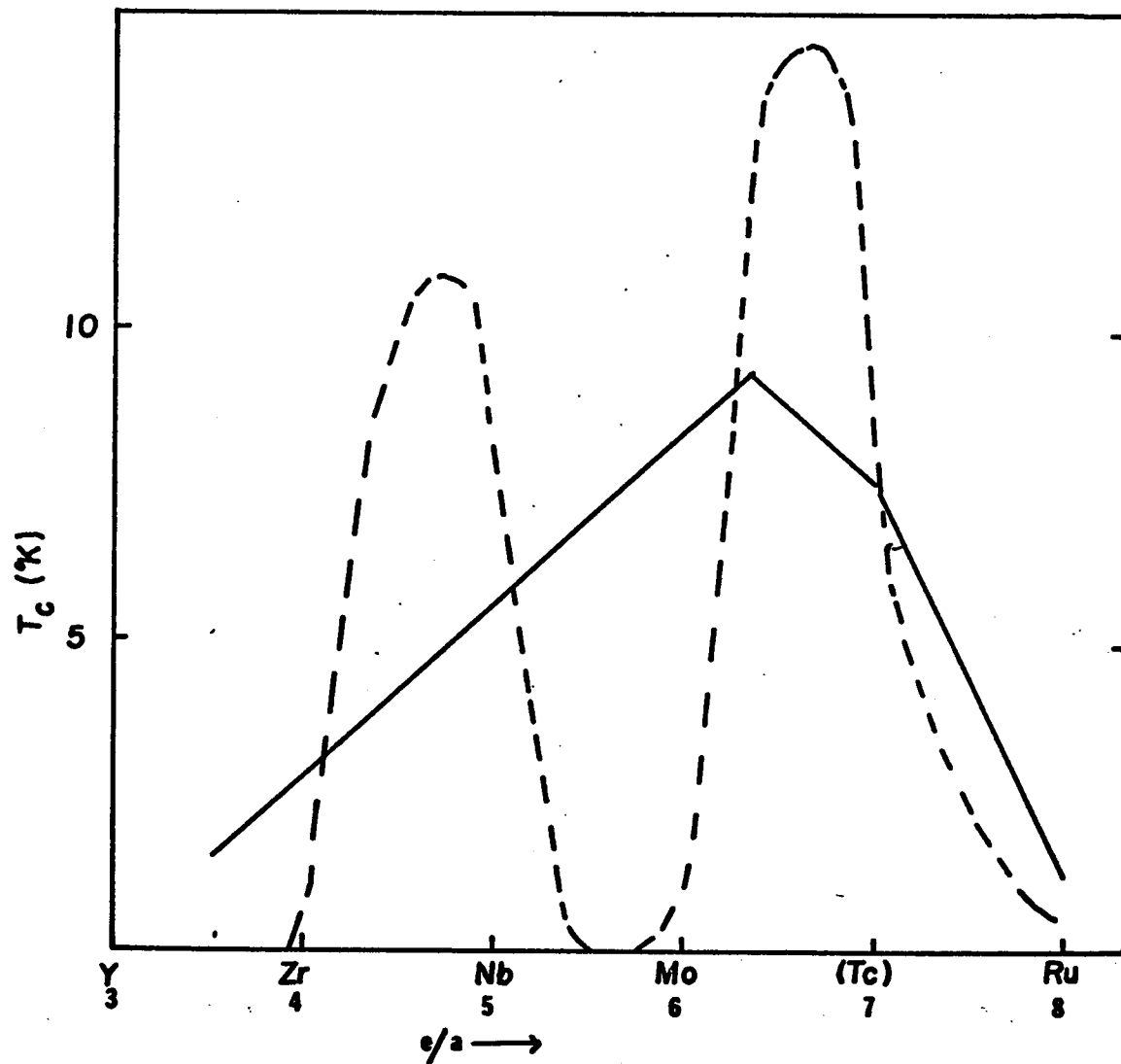


Figure 4. Superconducting transition temperature of the as-deposited vapor quenched 4d transition metal films versus the number of electrons per atom. The dashed line is for crystalline state and the solid line for the amorphous state. This is taken from reference 22.

$N(E_F)$  where it exhibits maxima (near Nb and Ta) and increasing  $N(E_F)$  where it exhibits minima (near Mo and W).<sup>28</sup> Collver also indicated that other types of smearing or alterations are possible which would strongly alter  $N(E_F)$ . These include a smearing due to a variation in the number of nearest neighbors, and alteration of the effects of s-d and d-d hybridization due to the loss of symmetry and change of short range order. The form of short range order, i.e., the number of nearest neighbors and their interatomic spacing, will introduce a "band structure" all its own. This short range order will tend to be close packed, i.e., an h.c.p. or f.c.c. structure (including V, Nb, Mo etc.)<sup>22</sup>.

Snow and Waber<sup>29</sup> made the band structure calculation for 3d transition metal series assuming that they take up f.c.c. structure and obtained a  $N(E_F)$  for f.c.c. with less large scale variation than for the b.c.c. structure. Furthermore the entire band shape i.e.,  $N(E)$  versus  $E$  takes on a broad single peak behavior to a first approximation, especially if one favors the  $s^2d^{n-1}$  over  $sd^n$  configuration in the solid. According to Snow and Waber the  $s^2d^{n-1}$  is to be preferred since the Fermi level and energy states lie at the larger energy in  $sd^n$  configuration. This is a reflection of the electrostatic repulsion between d electrons.

From these theoretical considerations, we will see the following points pertinent to the NMR study of both the amorphous and the crystalline VZr alloy: Firstly, Friedel oscillations account for the linewidth and the change of Knight shift even though detailed application of theory is impossible for these concentrated alloys.

Secondly a band theory cannot be ruled out. Only a small portion (~2%) of susceptibility  $\chi$  is highly sensitive to band changes and the lack of appreciable changes in Knight shift does not rule out changes such as Collver discusses.

### III. Experimental Procedure

In this section details of the preparation of the amorphous transition metal alloy VZr film will be discussed. This is followed by a brief discussion of the experimental apparatus used in the detection of the NMR signals.

#### A. Preparation of Samples

The VZr films were prepared by the RF sputtering process. Sputtering is a coating process which involves the transport of almost any material from a source, called a target, to a substrate of almost any material. The ejection of the source material is accomplished by the bombardment of the surface of the target with gas ions accelerated by high voltage. Particles of atomic dimensions from the target are ejected as a result of momentum transfer between incident ions and the target. The target-ejected particles traverse the vacuum chamber and are subsequently deposited on a substrate as a thin film. The main feature of the sputtering module used in this research is shown in Figure 5. The deposition took place in the sputtering chamber with the following conditions: (i) RF frequency 13.56 MHz, (ii) RF power 100 watts, (iii) Argon gas pressure  $3 \times 10^{-3}$  torr, and (iv) background pressure is  $1 \times 10^{-5}$  torr.

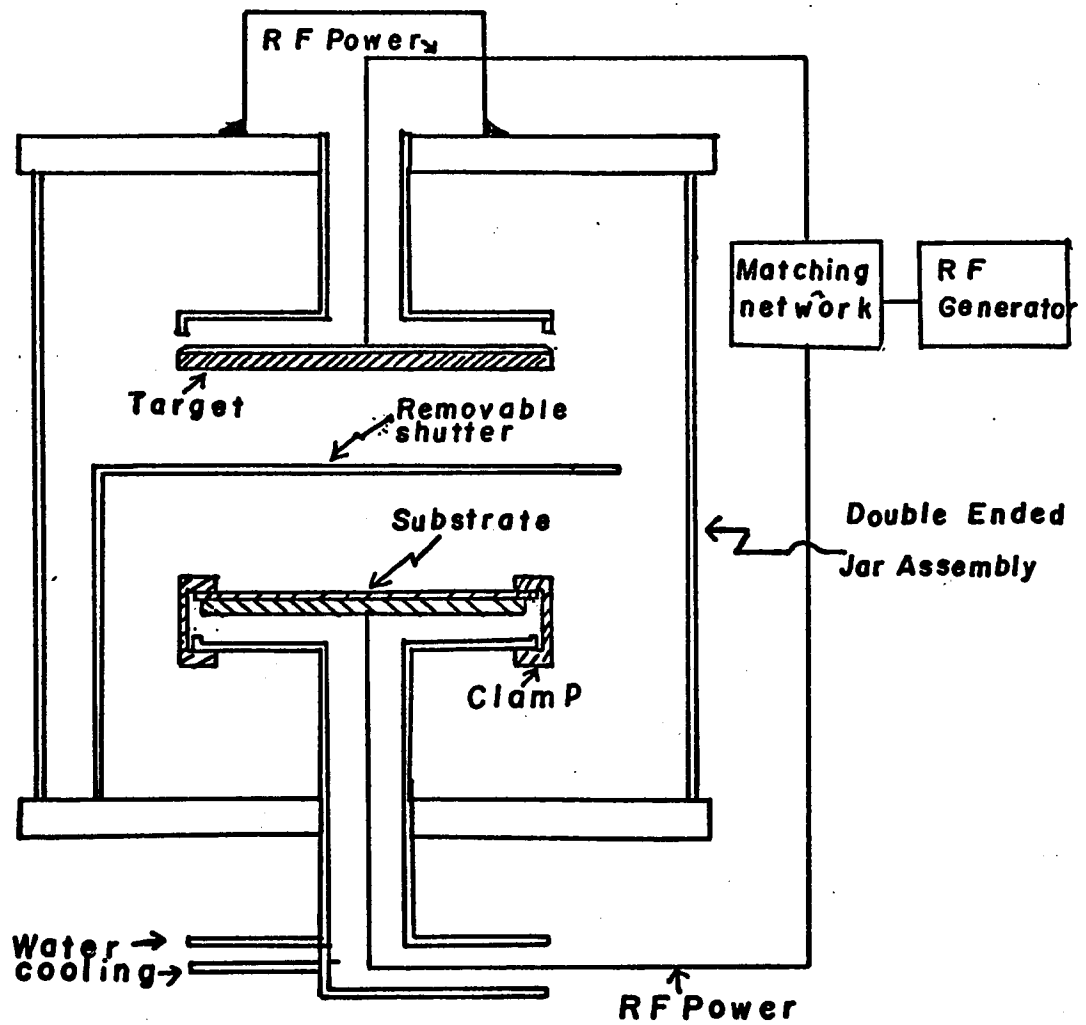


Figure 5. Schematic diagram of the Sputtering module

## B. Target and Substrate

To obtain VZr alloy films with various concentrations, five inch diameter discs of pure vanadium and zirconium were used with the following arrangements: In order to obtain a suitable Zr sputtering rate and uniform VZr film on a substrate, 61 holes were drilled onto a 5" diameter disc of the vanadium target. Then the vanadium target with 61 holes was sandwiched with the zirconium target so that this sandwiched target was exposed to the incoming argon ions as shown in Figure 5. The amount of zirconium concentration in VZr alloy film was dependent on the size of the holes in the vanadium target, because the size of the holes determined the area of zirconium target accessible to the incoming argon ions. For example,

Size of hole in vanadium target (in diameter)	Approximate Zr concentration in VZr alloy film
0.202"	10%
0.282"	20%
0.251"	30%
0.453"	40%

The films were deposited on a 5" diameter copper or aluminum disc (1/16" thick). The substrate was then mounted in a substrate holder and clamped directly against the water-cooled copper plate as shown in Figure 5.

## C. Structure and Composition Analysis of VZr Film

The structure of the sputtered VZr film was determined by

X-ray diffraction. In order to eliminate X-ray diffraction patterns due to copper or aluminum substrate, X-ray diffraction of the substrate was taken. Using the following formula<sup>30</sup> (Scherrer formula),

$$t = 0.9\lambda/B \cos \theta$$

where  $t$  = grain size,  $\lambda$  = wavelength of X ray used,  $B^2 = B_M^2 - B_S^2$  ( $B_M$  = the measured half width of X-ray intensity peak for the sample,  $B_S$  = the measured half width of the standard), one can obtain the approximate grain size of VZr alloy film. The amorphous VZr<sup>17.2</sup>, VZr<sup>28</sup> and VZr<sup>46.4</sup> films (where the superscript denotes the Zr<sup>91</sup> concentration, in atomic percent) give about 10 Å as upper limit for the grain size. Other films show the crystalline phase, and their grain sizes are larger than a few thousand angstroms.

The composition of binary alloy films is determined by both Rutherford back scattering spectrometry<sup>31</sup> and neutron activation analysis<sup>32</sup>. The Rutherford back scattering spectrometry uses the following principle. When a collimated beam of monoenergetic helium ions or of another light element impinges on a target, some of the helium particles are reflected by elastic collisions with the atom of target. The scattered particle loses energy in amount related to the mass of the atom struck. Further, the number of particles so scattered is a function of the number of atoms present. Hence by measuring the number of the emerging particles, the identity and number of atoms in the film can be determined. The relationship between the number of atoms  $N_A/cm^2$  present in a target and the number of scattered particle  $n_a$  detected will be given by

$$n_a = ((M_A - m) / (M_X + m))^2 Z_A^2 N_A,$$

where  $M_A$  is the mass of type A atom in the target,  $m$  the mass of helium atom and  $Z_A$  the atomic number of type A atom. Similarly for the type B atom,

$$n_B = (M_B - m/M_B + m)^2 Z_B^2 N_B.$$

Hence the relative number of type A and B atom present in a film will be given by

$$\frac{N_A}{N_B} = \left( \frac{M_B - m / M_B + m}{M_A - m / M_A + m} \right)^2 \left( \frac{Z_B}{Z_A} \right)^2 \frac{n_A}{n_B}.$$

The  $n_A/n_B$  is evaluated directly from the observed energy spectrum.

The results of these measurements are shown in Table I.

Table I.

the original estimates from the area of hole size.	Rutherford backscattering method	Neutron activation analysis.
V-Zr <sup>5</sup>	V-Zr <sup>6.4</sup>	V-Zr <sup>8.5</sup>
V-Zr <sup>10</sup>	V-Zr <sup>8.4</sup>	V-Zr <sup>20.6</sup>
V-Zr <sup>20</sup>	V-Zr <sup>17.2</sup>	V-Zr <sup>30</sup>
V-Zr <sup>30</sup>	V-Zr <sup>28</sup>	V-Zr <sup>49.3</sup>
V-Zr <sup>50</sup>	V-Zr <sup>46.4</sup>	V-Zr <sup>75.8</sup>

The superscript denotes the atomic percent of zirconium. The experimental error in Rutherford backscattering method will be less than 0.5%. Neutron activation analysis for the Zr<sup>91</sup> concentration in VZr film was performed by the nuclear engineering department at VPI and State University. They claimed the accuracy of the analysis was low, because the background activity of the copper substrate was high.

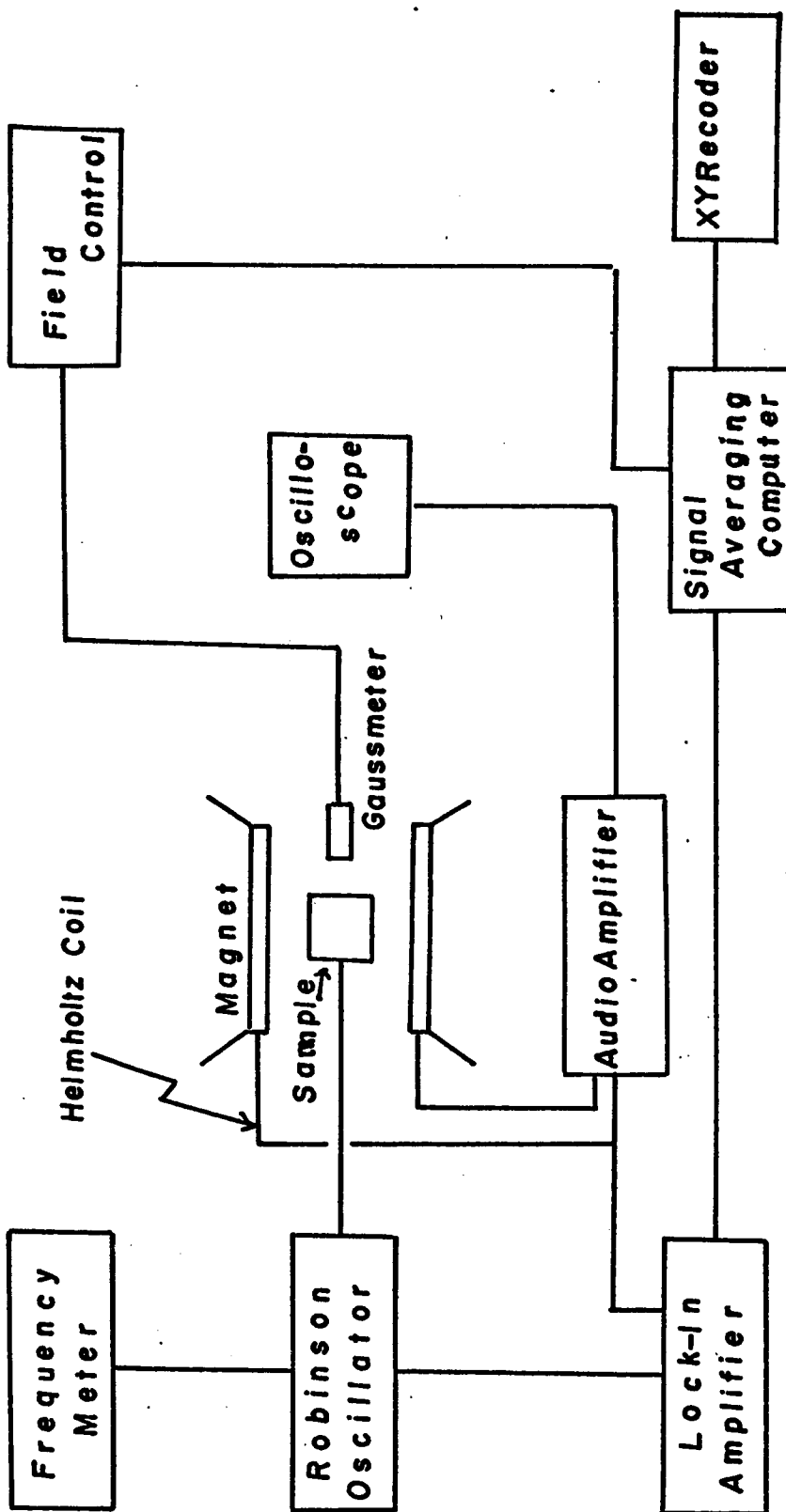


Figure 6. Block Diagram of NMR System

#### D. NMR Equipment

As NMR spectrometer, the Robinson oscillator<sup>32</sup> was used for obtaining the data. This is one of the standard CW NMR detection systems, and will be discussed below.

A block diagram of the NMR system is shown in Figure 6.

Robinson oscillator consists essentially of a variable R. F. frequency oscillator operated under such conditions that a decrease in  $Q$ , occurring as the frequency or the field is swept through the nuclear magnetic resonance, causes a decrease of the level of oscillation. The sample whose NMR is to be observed is placed directly inside an rf coil which is a part of the tank circuit of the oscillator. When the sample absorbs rf energy at resonance, this represents a decrease in  $Q$  in the tank circuit, and the change in the level of oscillation may be observed by measuring the rf voltage across this sample bearing coil. The advantages of both Robinson and Pound-Knight-Watkin's (PKW) marginal oscillator are as follows: (1) since they respond to changes in resistance only, the resonance line is due entirely to  $\chi''$ , the absorptive part of the effective susceptibility (except with single crystals or large sample grains, where eddy current mixing of  $\chi'$  and  $\chi''$  occurs); (2) they are readily adaptable to placing the sample directly into a variable temperature system -- the sample coil is merely soldered to a coaxial cable by which it is suspended inside the dewar vessel.

The Robinson oscillator circuit that was used in this study was modified by Petrinovic<sup>33</sup> and is shown in Figure 7 and 8.

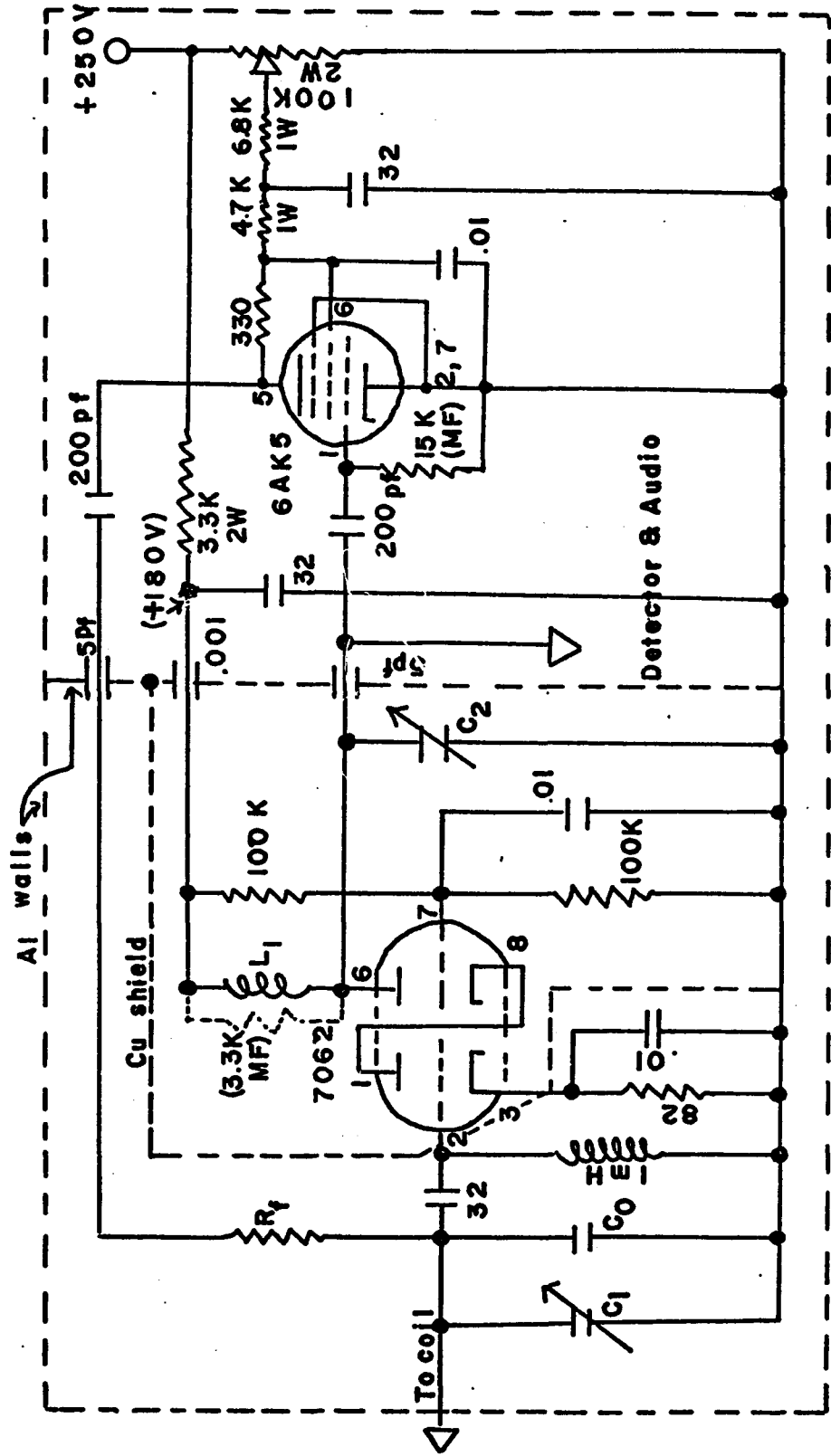


Figure 7. Robinson Oscillator and Limiter Circuit

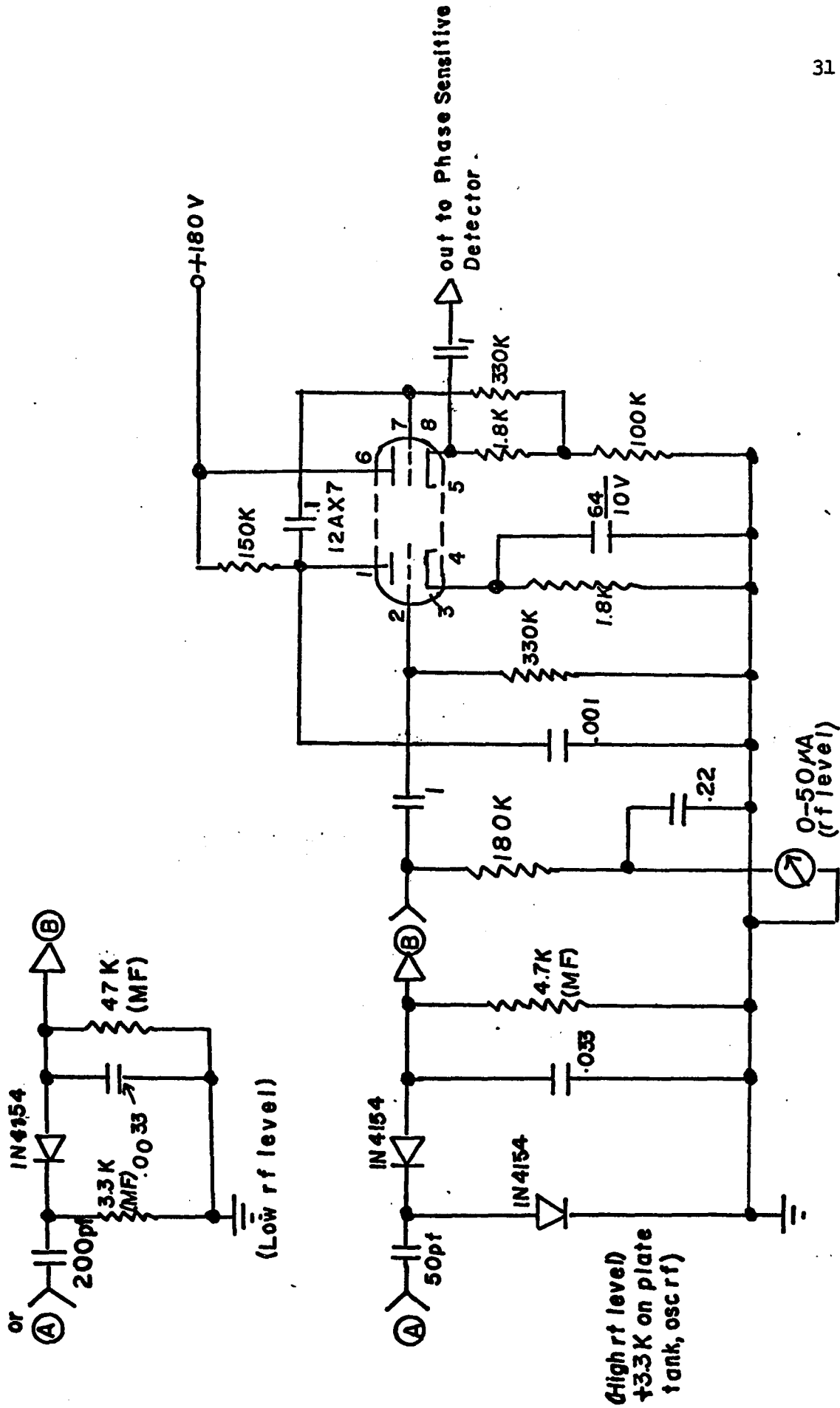


Figure 8. Detector and Audio Sections for Robinson Circuit

According to Howling's<sup>34</sup> analysis of the signal and noise characteristics of Robinson circuit, the signal response in the Robinson circuit rises with an increase in rf level for all modulation frequencies. In the PKW unit the response rises and falls in a manner determined by the modulation frequency and the AVC feedback constant, as described by Watkin's<sup>35</sup> theory. Furthermore in the Robinson circuit, the oscillation gain is constant and the effective feedback factor (limiter) controls the rf level. Oscillator mixing is, therefore, not influenced by rf level in the Robinson unit, but the mechanism of noise generation by shot noise mixing is the same for both the Robinson and PKW unit. Another virtue of the Robinson oscillator is the stability of operation at low rf level oscillation, because the limiting is done at high level so that there is, in principle, no lower limit to the level at the nuclear resonance coil. On the other hand the disadvantages of PKW oscillator are threefold. Firstly, it is more sensitive to microphonics; secondly, it is difficult to adjust at very low level; and finally it cannot be used with a circuit of low L/C ratio. All the disadvantages of PKW stem from the use of one tube to provide both regeneration and amplitude limiting. In the Robinson circuit these functions are separated.

#### E. General

NMR spectrometers, in general, use standard narrow-band detection techniques employing the lock-in amplifier. The use of such a phase sensitive detection scheme is dictated primarily by the

low signal to noise ratio of NMR signals in solids. This requires magnetic field modulation. The reference signal from the lock-in amplifier, after amplification by an audio frequency amplifier, is fed to a pair of Helmholtz coils attached directly to the pole pieces of the magnet. A frequency on the order of 100 Hz is typical. If this modulation amplitude is small compared to the NMR absorption line width, one obtains at the output of the lock-in a signal proportional to the derivative of the absorption line. This is illustrated in Figure 9.

Because NMR lines from the samples used here have a very low signal to noise ratio, a signal averaging computer (Northern Scientific Model 560) was employed to improve the NMR signal. In signal averaging measurement, the signal function, composed of both the desirable signal component and an undesirable component, usually noise, is synchronized to the sweep of a signal averager by a time-locked trigger command. The amplitude of the signal function is sampled periodically, digitized, and added to the memory of the averager. As the number of repetitive field sweeps increases, the desired component of the signal function accumulates in a linear manner while the noise component, which is random in nature, contributes both positive and negative component to the accumulated results in random manner and therefore at a rate equal to the square root of the number of sweeps performed. The direct "square root" relationship is strictly valid only for Gaussian distributed noise. However, even non random noise will be attenuated as long as it is not time locked to the signal component. The number of counts

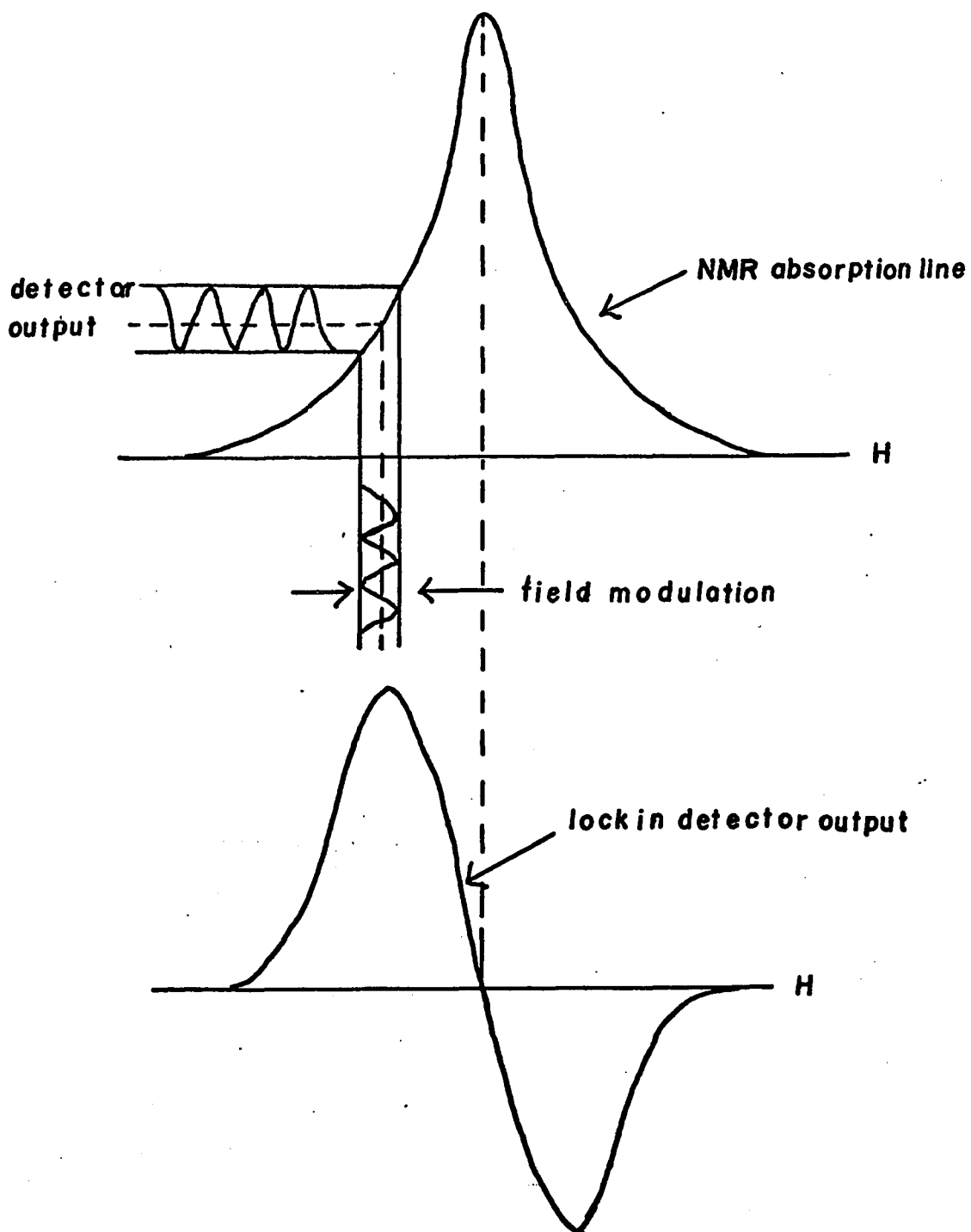


**Figure 9.** Illustration of the manner in which the derivative of the NMR absorption line is obtained by the use of field modulation small compared to line width.

accumulated in each address of memory after an arbitrary number of sweeps is equal to the average values of the sample signal function multiplied by the number of sweeps performed. In order to obtain a reasonable NMR signal line for the amorphous VZR films, about 10 to 14 field sweeps were required.

The electromagnet used with the Robinson oscillator system and the signal generator was a Magnion (model HSR 10200), capable of providing field from 0 to 30 KG. It has 15" pole pieces tapered to 6", with a 1 3/4" gap, just large enough to permit the Helmholtz coil to be placed directly on the pole faces and still allow room for the tail section of the low temperature dewar vessel. The sample bearing coil was placed directly in the cryogenic fluid -- either liquid helium or liquid nitrogen -- inside the inner dewar. By waiting until thermal equilibrium had been obtained, as could be determined by rf frequency stability, it was possible to be certain that the sample was at the same temperature as the coolant. Typically two or three hours were required to achieve thermal stability at liquid nitrogen temperature.

Field homogeneity was determined to be better than 0.1 gauss over the sample volume of approximate 2 cubic centimeters. In order to detect any field variation and field sweep rate change during the scan of NMR line, a NaCN reference, which was suspended just outside the dewar, was utilized. The sodium NMR line was run prior to recording the amorphous NMR line by the repetitive magnetic field sweep, and again immediately afterwards.

To eliminate time constant effects that tend to displace the line from its true position, three or more measurements of NMR lines were made. Since care was taken to employ sufficiently low sweep rates, well within the requirement of the 10 second output time constant of the lock-in amplifier, the averaging procedures give reliable results. Modulation effects on linewidth and shape were minimized by using as low a value of field modulation as signal to noise ratio permits, typically about 1/4 of the line width. It is estimated that error in the NMR line width is less than ± 5% for data obtained at 77°K.

#### IV. Results and Discussion

The data on the frequency shift and line width at 77°K for VZr films as sputtered on the copper or the aluminum substrate, and for the annealed VZr films are presented in Table II. Table III shows the relative intensity of NMR line between the amorphous state of VZr film and the crystalline state after annealing. The Knight shift change,  $\Delta K/K$ , relative to pure vanadium metal, whose Knight shift is 0.56%, is expressed in percent at a given external magnetic field. All line widths are the experimental peak to peak width of the observed absorption derivative.

##### A. Knight Shift

Figure 10 shows the change in Knight shift  $\Delta K/K_v$  versus Zr concentration for a series of VZr alloy films. Although the solubility limit of Zr in  $V^{36}$  is about 2 atomic percent at room temperature,  $VZr^6$  and  $VZr^{8.4}$  films in this figure were b.c.c. crystalline according to X-ray diffraction analysis. The  $VZr^{17.2}$ ,  $VZr^{28}$ , and  $VZr^{46.3}$  samples were amorphous. (The superscript denotes the Zr concentration in V, in atomic percent.) The estimated errors in the observed Knight shift never exceeded  $\pm 5\%$  of the measured values. The error bars are omitted from the figure in the interest of clarity.

Although all the observed changes of Knight shift were quite small, we can make the following observations. The addition

TABLE II

## Knight Shifts and Line Widths

	H=8 KG		H = 11 KG		H - 13.5 KG		H=17 KG	
	$\Delta K/K_v\%$	$\Delta\nu(KHZ)$	$\Delta K/K_v\%$	$\Delta\nu(KHZ)$	$\Delta K/K_v\%$	$\Delta\nu(KHZ)$	$\Delta K/K_v\%$	$\Delta\nu(KHZ)$
V(pure)	0	11.8	0	12	0	12.6	0	13.2
VZr <sup>6.4</sup>			-1.5	16.4			-2.4	20
VZr <sup>8.4</sup>	-2.0	16	-2.2	18.6	-1.8	21	-3.1	25
VZr <sup>17.2</sup>	-2.1	16.8	-2.8	19.8	-3.2	22.4	-4	26
VZr <sup>28</sup>	-2.2	17	-2.9	19	-3.0	20	-4.2	23
VZr <sup>46.4</sup>	-2.5	16.8	-3.2	19.2	-3.5	20.8	-4	23
VZr <sup>17.2</sup>	+1.2	16.1	+0.6	18.8	+0.9	20.6	-0.6	24.8
(annealed to 460°C)								
VZr <sup>28</sup>	-1.1	13.7	-1.5	14.4	-1.2	14.5	-1.0	15.4
(annealed to 900°C)								
VZr <sup>46.4</sup>	-2.0	12.8	-1.6	13.6	-1.1	14.2	-0.9	14.7
(annealed to 900°C)								

Table III

Relative line intensity of VZr film between the amorphous state and the crystalline state (the annealed one)

	H = 11 KG	H = 13.5 KG	H = 17 KG
	Relative Intensity	Relative Intensity	Relative Intensity
	$Jx(\Delta v^2)/J_o x(\Delta v_o^2)$	$Jx(\Delta v^2)/J_o x(\Delta v_o^2)$	$Jx(\Delta v^2)/J_o x(\Delta v_o^2)$
VZr <sup>28</sup>	.18	.16	.21
VZr <sup>46.4</sup>	.19	.22	.30

J = amplitude of the absorption line for the amorphous film

J<sub>o</sub> = amplitude of the absorption line for the annealed film

$\Delta v$  = line width of the amorphous film

$\Delta v_o$  = line width of the annealed film

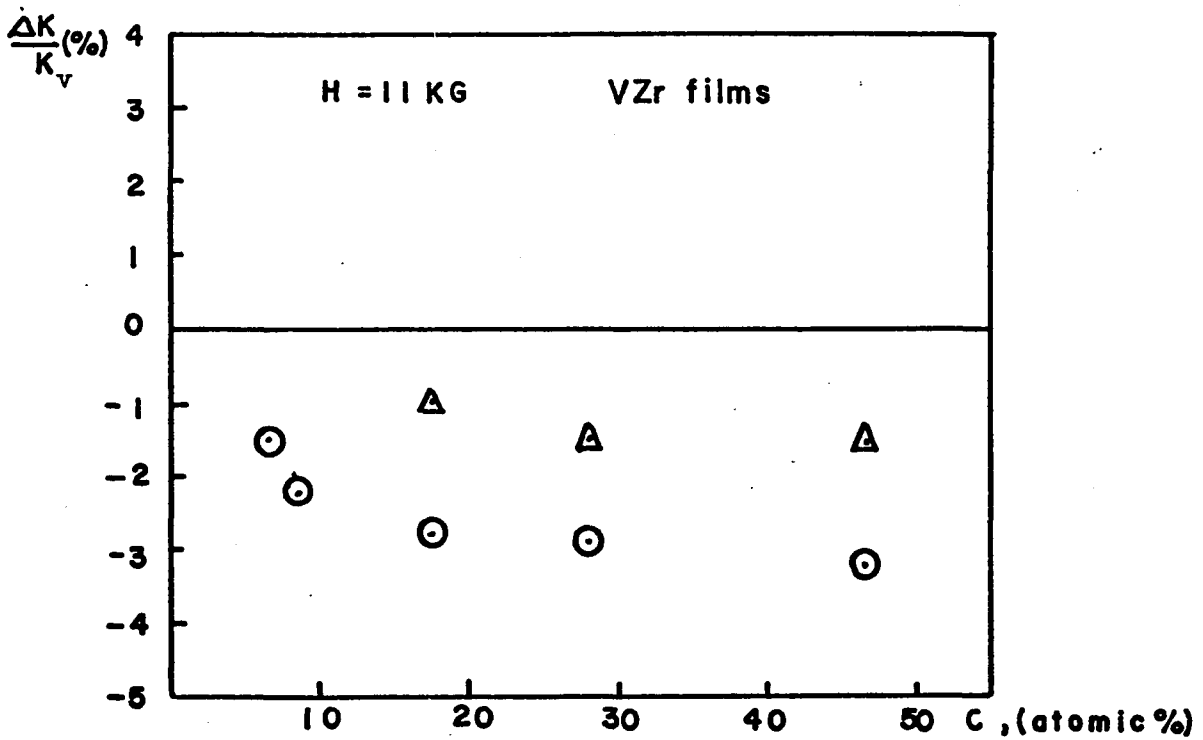
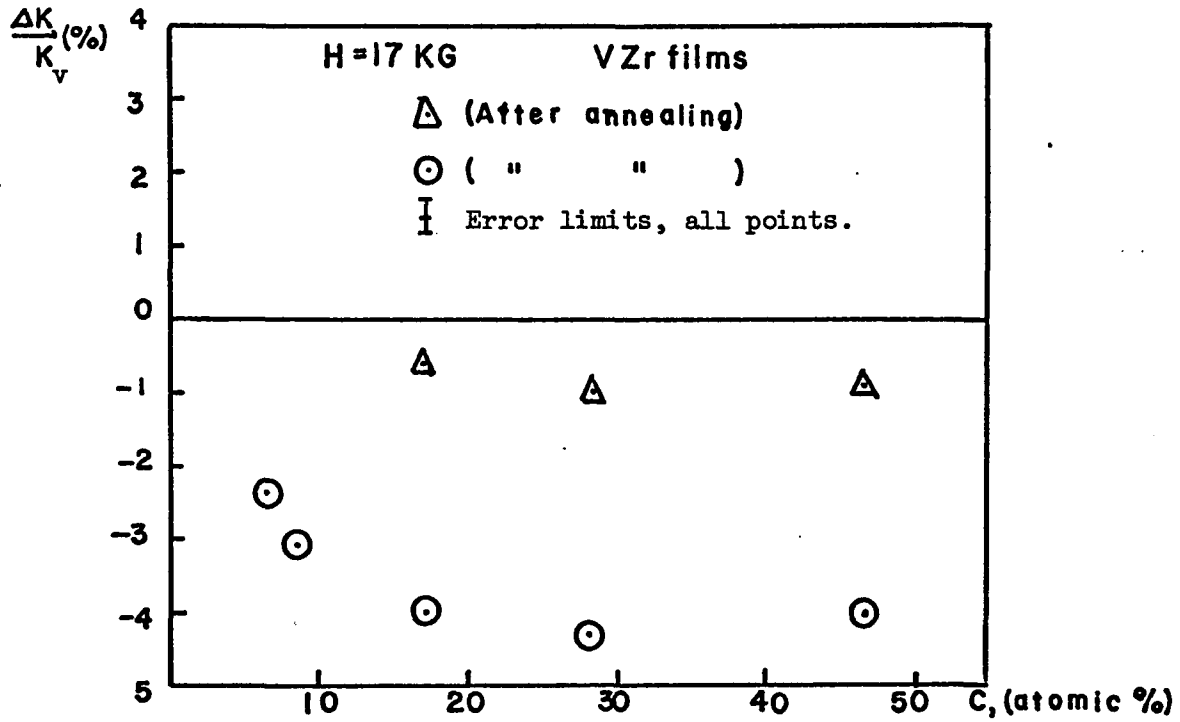


Figure 10.  $\Delta K/K_V$  versus Zr concentration, VZr alloy

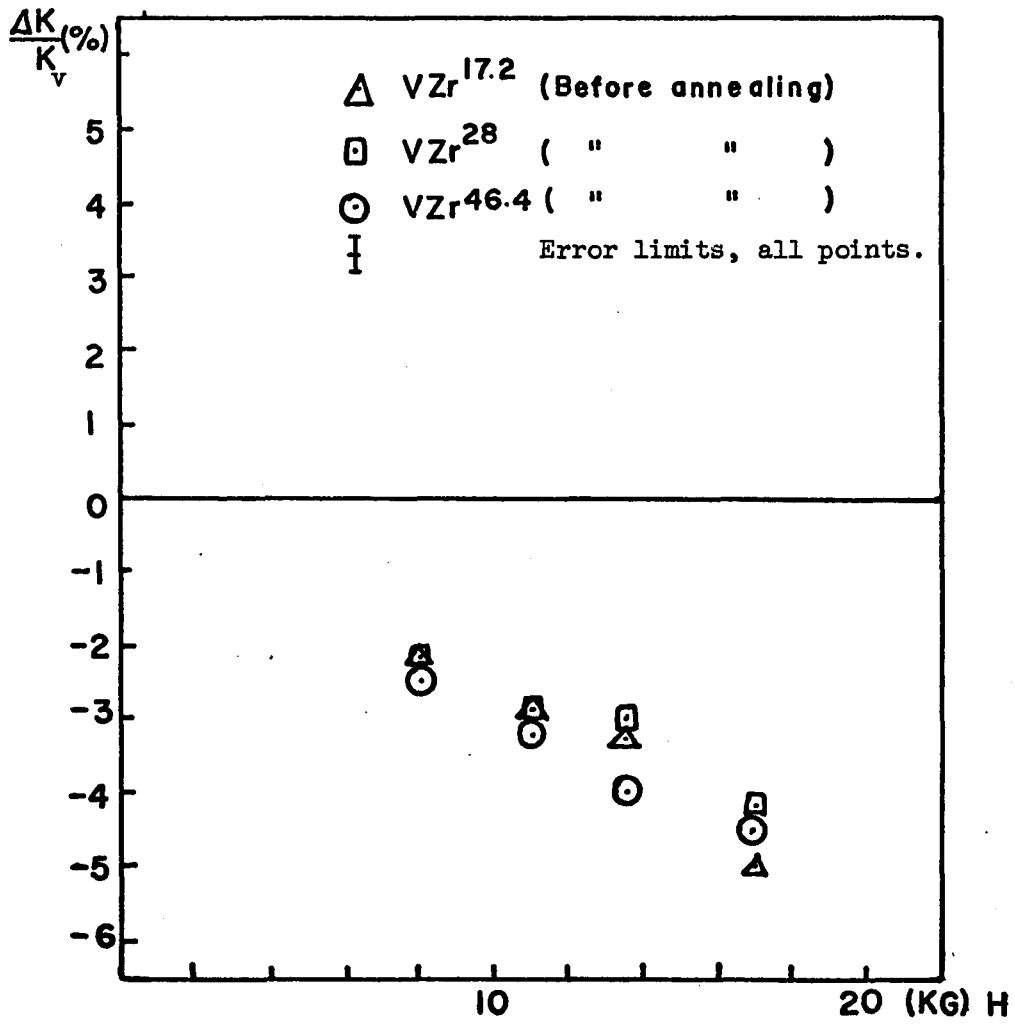


Figure 11.  $\Delta K/K_v$  versus field H, VZr alloy (amorphous phase)

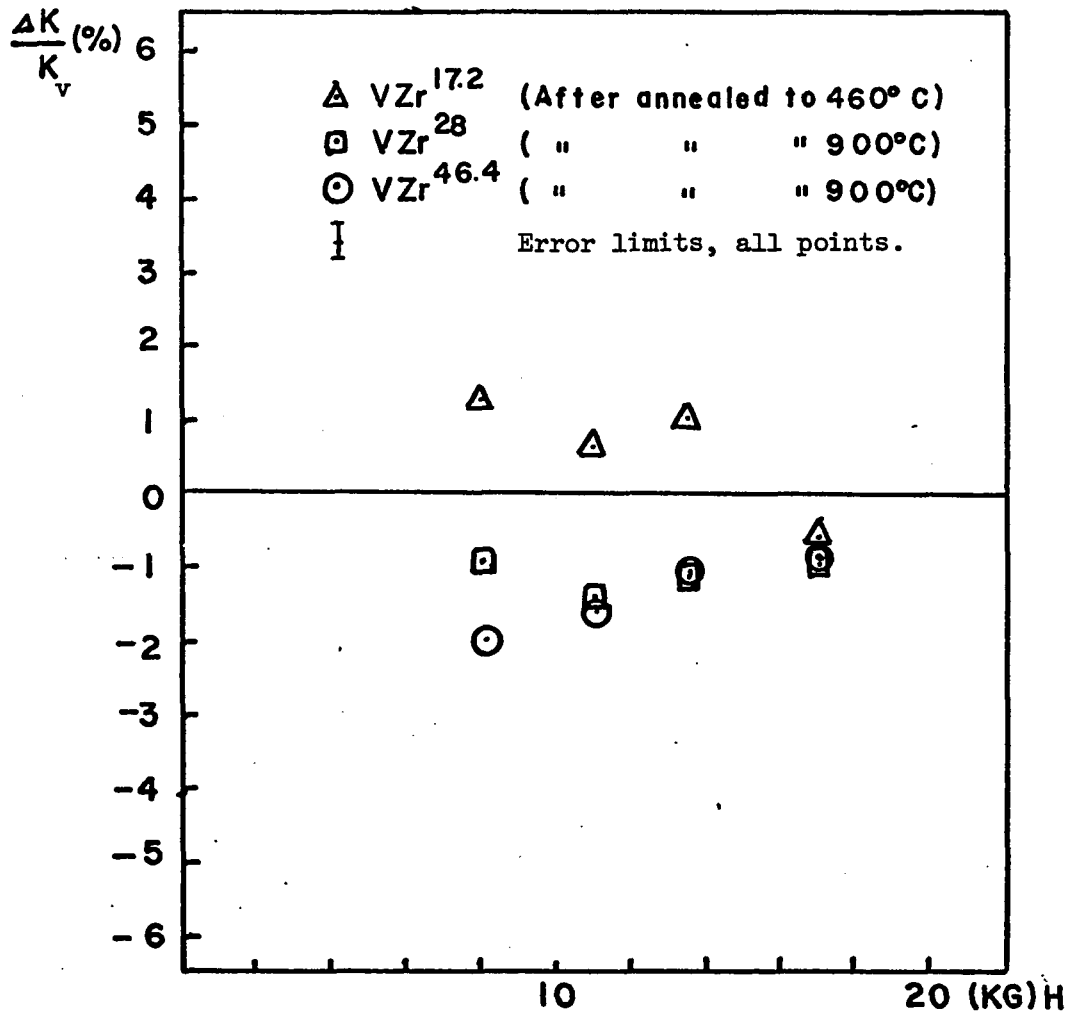


Figure 12.  $\Delta K/K_v$  versus field H, VZr alloy

of zirconium to vanadium decreases the Knight shift relative to the pure vanadium until the VZr alloy film becomes amorphous. Then the decrease of Knight shift remains almost constant for the amorphous phase of VZr films whose Zr concentrations are larger than 17.2%. Since we did not anneal VZr alloy film with the lower Zr concentration, it is difficult to predict whether there exists any additional change in Knight shift by annealing. On the other hand annealed VZr films from their amorphous phase show only a negligible decrease of Knight shift relative to pure vanadium. This indicates that the Knight shift of the annealed VZr films, which were transformed to the crystalline phase from the amorphous one, is not sensitive to Zr concentration.

Figure 11 and 12 show the change of Knight shift versus the external magnetic field  $H$  before and after annealing the amorphous VZr films. They show that the Knight shift of VZr film in the amorphous phase has a tendency to decrease linearly as the field  $H$  increases. The VZr<sup>17.2</sup> film, which was annealed to 460°C because of the low melting point of an aluminum substrate, still shows a linear decrease of Knight shift as the field  $H$  increases. This is because the annealed VZr<sup>17.2</sup> film is still in a metastable phase. However, the VZr<sup>28</sup> and VZr<sup>46.4</sup> films after annealing to 900°C show that their Knight shifts remain constant independent of  $H$  and  $\Delta K \sim 0$  within the experimental error. This is a marked contrast in the behavior of Knight shift between the amorphous phase and the crystalline phase of VZr alloy film.

The decrease of Knight shift in VZr film as a function of the field  $H$  and Zr concentration may be attributable to the long

range oscillations of electronic charge density believed to exist around the impurity. We have not attempted to calculate the effect of the oscillations of the charge density for VZr alloy using Blandin-Daniel's theory, which predicts a linear relation of Knight shift to the concentration because the exact phase shifts which describe the scattering process in this theory are unknown. The simplifying assumptions involved become more questionable for the transition metal.

Alternatively the dependence of Knight shift of  $V^{51}$  on the lower Zr concentration may be described in terms of the rigid band model mentioned in the previous section. In this model, the alloying elements which are neighbors in the periodic table simply increase or decrease the number of electrons in the band without having appreciable effect on the form of the band. Thus if one believes the rigid band model, then the decrease in the Knight shift of  $V^{51}$  in VZr film until Zr concentration reaches about 8.4% may be attributable to the decrease of s-electrons and the increase in the density of states in the d-band. Since the rigid band model<sup>1</sup> assumes that an alloy has almost the same electronic band structure as that of the pure host metal and that each impurity with screening cloud of electrons is far from others, this model is not applicable to an amorphous VZr alloy where  $Zr^{91}$  concentration is high.

A possible explanation for both the near constancy of Knight shift and the linear field dependence of Knight shift in the amorphous phase of VZr film is as follows: In the formation of the amorphous

phase of VZr film as sputtered, the gas molecules may be trapped in the interstitial or substitutional sites for the stabilization of the amorphous phase of VZr film<sup>37,38</sup>. Consequently, possible changes in the shape of the density of states curve, variation in the Fermi level and large electric field gradients will be produced. Because of the additional structural disorder introduced by the gas impurities, the long range oscillations of the electronic density around each impurity atom may overlap each other at the higher Zr<sup>91</sup> concentration. Therefore, the center of gravity of the relative variation of Knight shift may become insensitive to Zr concentration. For a theoretical estimate of the long range oscillation effect in amorphous VZr alloy, these effects also should be taken into consideration in Blandin-Daniel's theory for the calculation of the average Knight shift and the linear field dependence of the Knight shift.

#### B. Linewidth

As shown in Figure 13, the linewidth broadens rapidly as Zr is added to V<sup>51</sup>. At H = .11 KG the linewidth increases from 13.2 KHz in pure vanadium to about 20 KHz for the amorphous VZr<sup>17.2</sup> alloy film. For Zr concentration larger than 17.2%, the line width is almost constant in the amorphous phase.

As shown in Figures 14, 15 and 16 the linewidth in the amorphous phase of VZr depends linearly on the external field H, but the linewidth in the crystalline phase after annealed above 900°C is almost independent of the external field H. The possible contributions

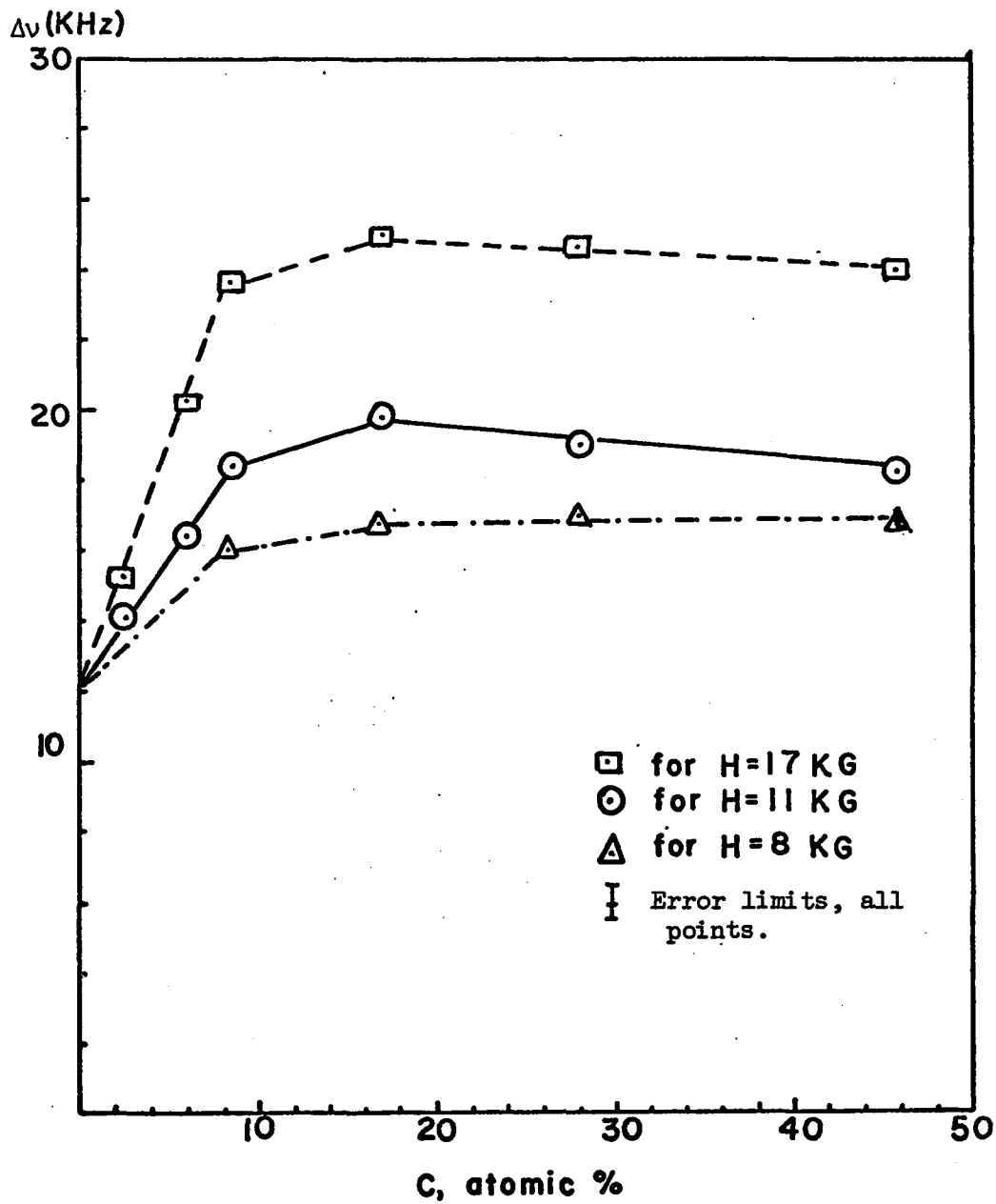


Figure 13. Linewidth of  $V^{51}$  versus Zr concentration, VZr alloy

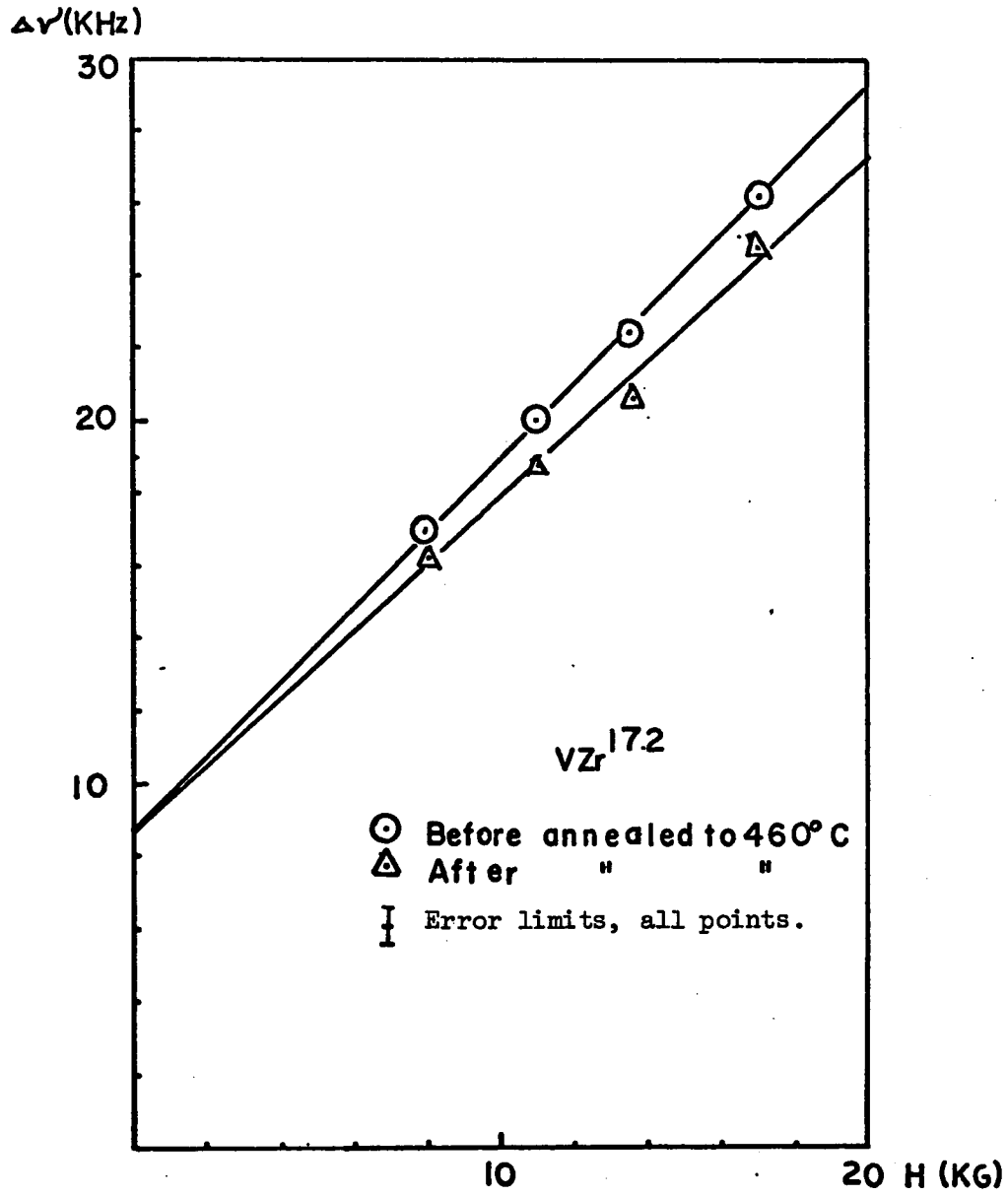


Figure 14. Linewidth of  $V^{51}$  versus field  $H$ ,  $VZr^{17.2}$  alloy

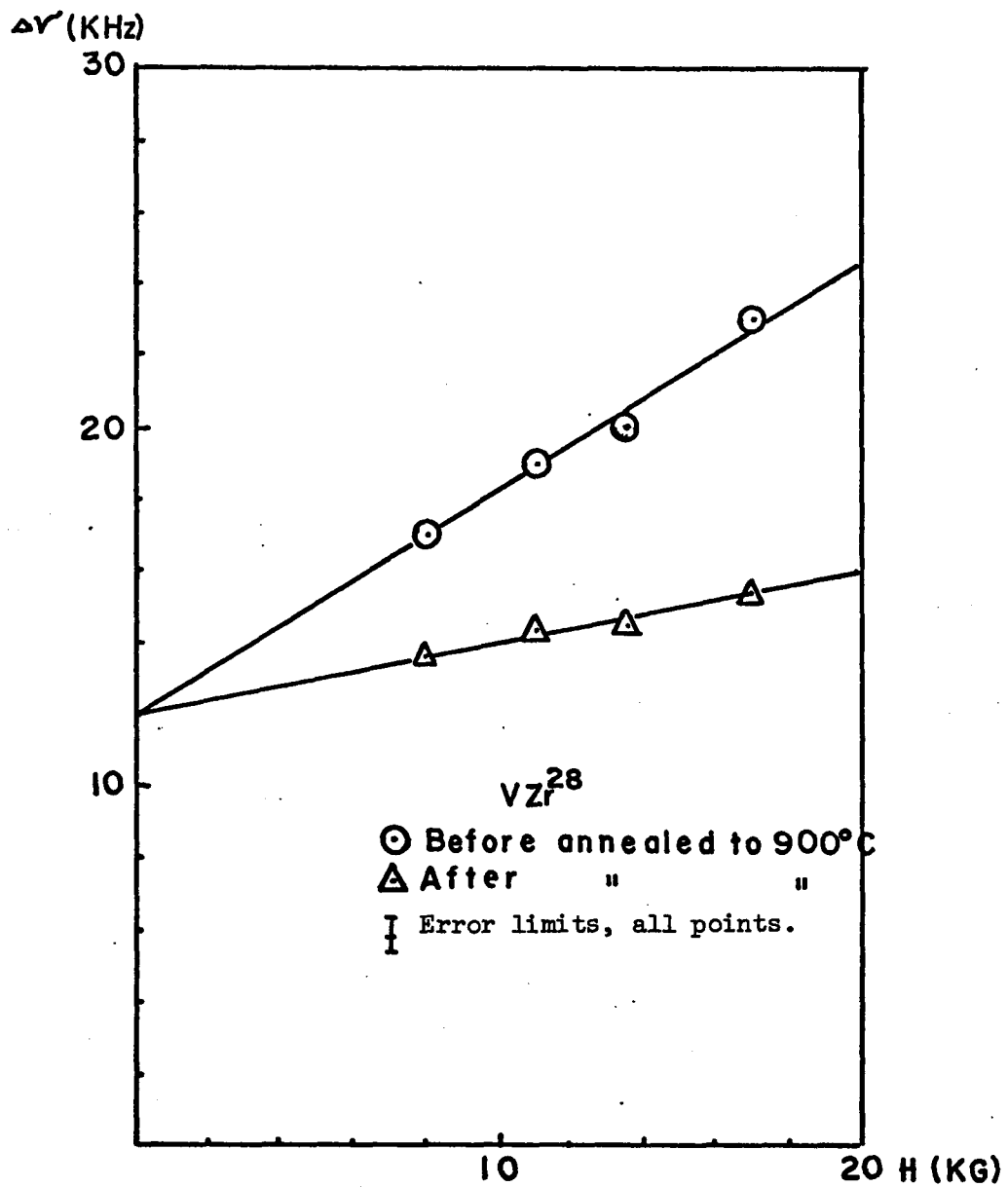


Figure 15. Linewidth of  $V^{51}$  versus field H,  $VZr^{28}$  alloy

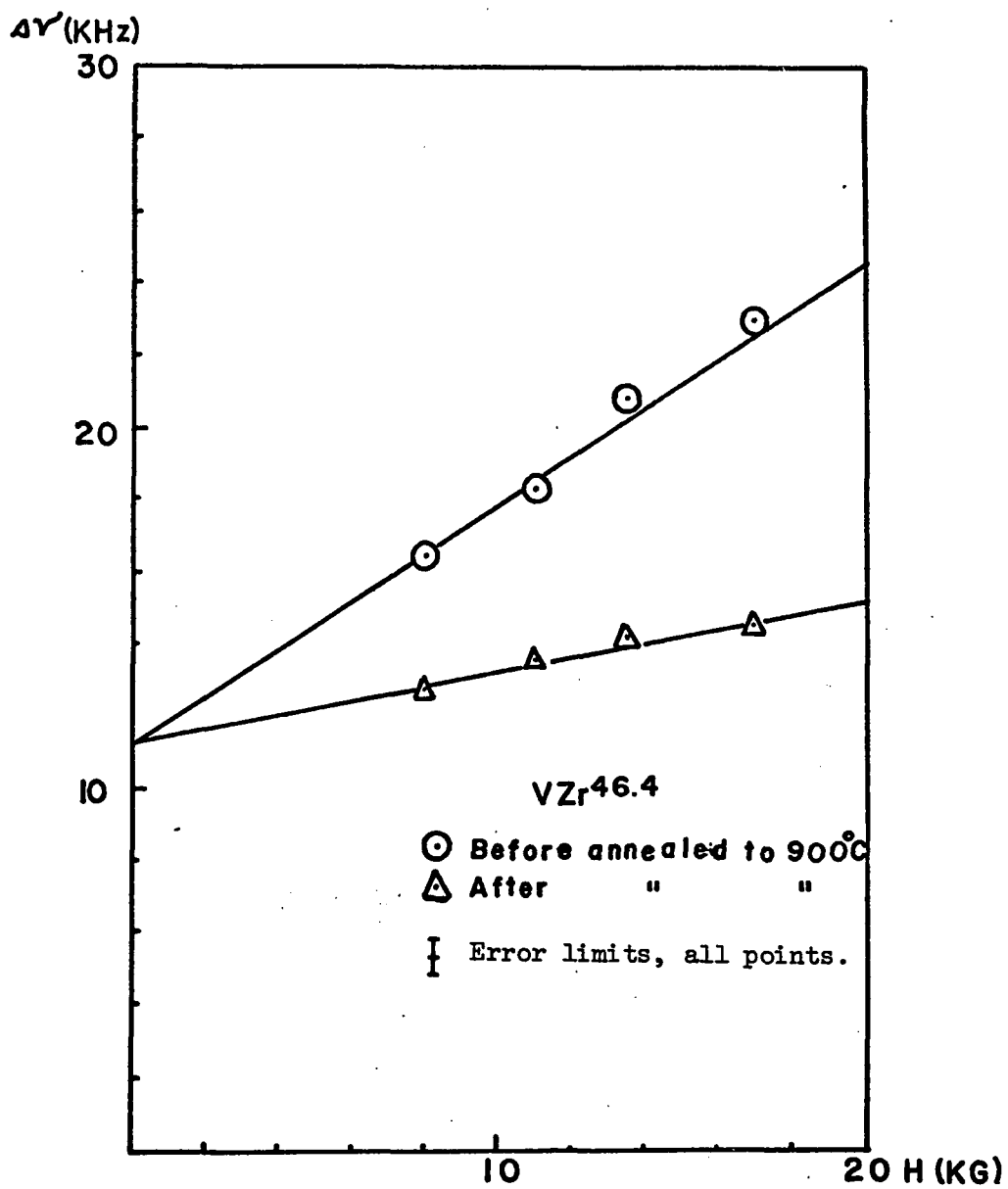


Figure 16. Linewidth of  $V^{51}$  versus field H, VZr<sup>46.4</sup> alloy

to the linewidth are the following: (1) the dipolar linewidth, (2) the indirect exchange broadening and pseudodipolar broadening, (3) the life time broadening, (4) macroscopic field inhomogeneities produced by the bulk magnetism of the sample, (5) inhomogeneous Knight shift broadening, (6) anisotropic Knight shift broadening, and (7) quadrupolar broadening. Among these possibilities (1) and (5) will give major contributions. The remaining (2), (3), (4) and (6) will give almost negligible contributions.

The dipolar linewidth is the portion of linewidth due to the magnetic dipolar interaction between nuclear magnetic moments. Using the Van Vleck<sup>39</sup> procedure, Kambe and Ollom<sup>40</sup> calculated the second moment of the central line of a magnetic resonance for half integral spin, for the case in which quadrupole coupling is present. They considered the interaction between resonant spins, the interaction between unlike spins, and the interaction between semilike spins. Here, resonant spins are the same species of spin with the same quadrupole coupling. Semilike spins are the identical spins located at the different lattice sites where the values of the quadrupole coupling constants are different. For the purpose of comparing the linewidth of vanadium in VZr alloy at zero field with the theoretical root mean square width, we calculated the second moment of pure vanadium instead of the concentrated VZr alloy whose lattice spacing in b.c.c. structure is not available. The calculated dipolar width without exchange effect is 10.7 KHz under the interaction between the resonant spins and

9.2 KHz under the interaction between semilike spin. The measured linewidth at zero field is determined by extrapolating the linewidth versus the field curve for both the amorphous and annealed samples and are found to be 8.6 KHz, 12 KHz and 11.2 KHz for  $VZr^{17.2}$ ,  $VZr^{28}$  and  $VZr^{46.4}$  respectively. The zero field extrapolation of the linewidth may have an appreciable error because the estimated error in the measured linewidth is  $\pm 5\%$  and there is a lack of the measured linewidth data at lower fields. Nevertheless, the linewidth of  $VZr^{28}$  and  $VZr^{46.4}$  show a good agreement with the root mean square width of the pure V based on the interaction between the resonant spins. Therefore the excess linewidth above the zero field must be attributed to the field dependent broadening and other minor sources.

The indirect exchange broadening and pseudo-dipolar broadening arise from indirect interaction between the nuclear magnetic moments, the former mediated via the conduction electrons through the hyperfine contact interaction, the latter via the conduction electrons through the dipolar term in the hyperfine interaction. Indirect exchange has been treated by Ruderman and Kittel<sup>41</sup>, and pseudo-dipolar interactions were discussed by Bloembergen and Rowland<sup>42</sup>. Since these effects are not present in the pure  $V^{51}$ , it is expected that these effects are insignificant in the amorphous VZr alloy if they exist.

Life time broadening, sometimes called spin lattice relaxation broadening, is a consequence of the Heisenberg uncertainty relation and is significant in the event of very short spin lattice

relaxation time. Masuda<sup>43</sup> measured the spin lattice relaxation time  $T_1$  of vanadium in VTi system, and  $T_1$  was about  $8 \times 10^{-3}$  sec at 77°K. The corresponding linewidth of  $T_1$  is about 1/16KHz. Thus the  $T_1$  contribution gives a negligible error in the linewidth measurement.

The magnetization of the particle produces field inhomogeneities within the sample leading to an apparent broadening of the magnetic resonance line. The field inhomogeneities within the sample depend on the geometry and the orientation of the sample relative to the external magnetic field. If the external magnetic field is rotated from parallel to perpendicular to the face of a stack of 0.020" thick thin flat substrates (Al or Cu), where VZr alloy films were sputtered, the demagnetizing field will be varied from zero to maximum. Consequently the Knight shift and the linewidth will be varied with the relative orientation of the sample to the magnetic field. We have not attempted to measure the apparent line broadening and the Knight shift change due to the field inhomogeneities within the sample. Schreiber<sup>44</sup> measured the Knight shift for  $V^{51}$  and  $H^1$  in metallic  $VH^{0.66}$  due to the geometrical effect. He found a sizable variation of the proton Knight shift (+0.012% to -0.030%) due to the geometrical effect. Drain<sup>45</sup> estimated the linewidth contribution due to the macroscopic field inhomogeneities. Assuming the linewidth  $\Delta H$  to be twice the root-mean-square deviation of the internal field, he obtained  $\Delta H = 3\chi_v H^{\sim 1}$  gauss at  $H = 10$  KG for powdered samples of pure  $V^{51}$  where  $\chi_v$  = volume magnetic susceptibility and  $H$  is the external field. Thus, the average line

broadening due to macroscopic field inhomogeneities is small compared to the linewidths for both amorphous and crystalline phases of VZr film, which are on the order of 20 gauss.

The inhomogeneous Knight shift broadening refers to the field dependent broadening produced by the Friedel oscillation in the electronic charge distribution about the impurity in the alloys. Thus nuclei at various distances from the solute atom experience different electron densities and therefore, different Knight shifts. As Figures 15 and 16 have shown, the linear field dependence of the linewidth is much more pronounced in the amorphous VZr film than in the corresponding crystalline one. This indicates that the inhomogeneous Knight shift broadening will be the major source of line broadening in the amorphous phase of VZr film. On the other hand though inhomogeneous Knight shift broadening may be a source of broadening in the crystalline phase it would not be a major source, because we observe only a slight linear field dependence in the crystalline phase. The Van Vleck term puts an upper limit on this term.

According to Blandin-Daniel's theory discussed in the earlier section, the field dependent portion of the linewidth  $\delta H$  in the alloy without the other sources of broadening will be given by

$$\delta H = \left[ \left( \frac{\Delta K}{K} \right)^2 - \left( \frac{\Delta K}{K} \right)^2 \right]^{1/2} = \left[ \left( \frac{\Delta \rho}{\rho} \right)^2 - \left( \frac{\Delta \rho}{\rho} \right)^2 \right]^{1/2} \Delta H$$

where  $\Delta H$  is the absolute Knight shift, which is proportional to  $H$ , and  $\frac{\Delta \rho}{\rho}$  is the relative variation of the charge density around the impurity. Since the exact phase shifts that describe the scattering process in

this case are unknown, accurate quantitative calculation of the inhomogeneous Knight shift broadening is not possible. If Blandin-Daniel theory can be extended to the concentrated VZr alloy, the proportionality of the linear field dependence will be used as a measure of the deviation  $\Delta K$ , to a certain extent. In our case the measured proportionalities for the linear dependence of the linewidth against the field are 1.03 KHz/KG, 0.62 KHz/KG and 0.66 KHz/KG for  $VZr^{17.2}$ ,  $VZr^{28}$  and  $VZr^{46.4}$  respectively.

The anisotropic Knight shift broadening exists only if the local symmetry is lower than cubic. The possibility of anisotropic Knight shift broadening may not be ruled out in both the crystalline phase and the corresponding amorphous phase of the VZr alloy films, because there must exist some deviation from the local cubic symmetry at  $V^{51}$  sites produced by adding Zr atoms and the trapped gas molecules. The contribution of anisotropic Knight shift broadening in VZr alloy film will be very small, because the change of Knight shift itself in both crystalline and amorphous phases of VZr alloy films was very small.

### C. Quadrupole Effects

Table III shows the relative intensity of the absorption line between the amorphous phase and the crystalline phase after annealing to function  $g(\nu)$ , is  $\int_0^\infty g(\nu) d\nu$ . A change in the width of  $g(\nu)$  not accompanied by a change in the shape will, of course, change the amplitude J which

we should like to use as a measure of intensity. In order to compensate for this when determining the integrated intensity, we note that since  $g(\nu)$  is normalized, its maximum value  $g(\nu_{max})$  is proportional to  $(\delta\nu)^{-1}$ . The peak to peak amplitude of the observed derivative  $J$ , is then proportional to  $Ix(\delta\nu)^{-2}$  and consequently the total intensity  $I$  is proportional to  $Jx(\delta\nu)^2$ . Thus we used  $I=Jx(\delta\nu)^2$  as a measure of the relative intensity.

Since it is difficult to maintain all the experimental parameters constant during the measurements on both the amorphous and the crystalline phases of VZr film, some method of calibrating the intensity scale is always required. Thus, each complete intensity measurement consist of observing both the resonance of the sample under observation and a reference signal provided in the form of a standard sample whose resonance is recorded. In our case, it was almost impossible to obtain a suitable standard sample, which for convenience should have a strong resonance close to, but not overlapping, the resonance of  $V^{51}$ . Therefore, the measured absorption line intensity of  $V^{51}$  in both the amorphous and the crystalline phases of VZr film could not be calibrated. However, we did not detect any change in the line shape.

The sharp decrease in the intensity of the vanadium NMR line in the amorphous phase relative to the crystalline phase may be attributed to the structural disorder on the atomic scale that introduces a large electric field gradient around the solute of  $Zr^{91}$  atom, and to the gas impurities in the interstitial sites. We assume that the electric field gradient is very large near a solute atom ( $Zr^{91}$  or a trapped gas

molecule) so that the resonance of any solvent  $V^{51}$  close to a solute atom will be unobservable. The solvent  $V^{51}$  atoms at greater distance from the solute have their central transitions effectively unperturbed and will clearly contribute their full share to the observed intensity. All  $V^{51}$  atoms which are within a critical distance  $R$  of a solute atom do not contribute to the resonance signal. If we denote the number of lattice sites within the radius  $R$  by  $n$ , then this leads to the following concentration dependence of the intensity:  $I = I_0(1-C)^n$  where  $C$  is the atomic concentration of solute.<sup>18</sup> Meerwall and Rowland<sup>21</sup> recently found that quadrupole effects in the  $V^{51}$  based alloy were several times smaller for transition metal (substitutional) solutes than for the substitutional oxygen and nitrogen impurities in vanadium. They obtained wipeout number  $n = 126 \pm 7$  for  $N$  in  $V^{51}$  and  $n = 194 \pm 12$  for  $O$  in  $V^{51}$  when all or nothing model was applied to the interstitial alloys. They also suggested from the solute dependence that the field gradients around the substitutional atoms arise mainly in response to local lattice distortion rather than to the shielding of the excess charge of the solute. We have not calculated the wipeout number of  $V^{51}$  atoms due to Zr atoms and gas impurities, because we have not measured the concentration dependence of satellite intensity. Although more accurate measurements of the absorption intensity for both the amorphous and crystalline VZr alloy film are required to make a comparison between experimental results and theory, the reduction of the intensity in the amorphous VZr alloy relative to the crystalline phase

appears to fit into the all or nothing model.

In conclusion, no significant changes in the behavior of Knight shift of  $V^{51}$  have appeared as the result of the phase transition from the crystalline state to the amorphous state, while the linewidth of  $V^{51}$  in the amorphous phase greatly increases relative to the crystalline phase. Furthermore, the intensity of the absorption line of  $V^{51}$  for the crystalline VZr alloy, after being annealed above  $900^{\circ}\text{C}$ , considerably increases relative to the amorphous phase.

The generally small value of the change in Knight shift of  $V^{51}$  upon the addition of small  $Zr^{91}$  concentration (less than 17%) appears to be consistent with the prediction of either the Friedel oscillation theory of Blandin-Daniel or rigid band picture proposed by Watson, Bennett and Freeman.<sup>46</sup> The small linear field dependence of Knight shift of  $V^{51}$  in the amorphous phase of VZr alloy indicates the possible existence of charge oscillations around the impurity. Furthermore, the linear field dependence of the linewidth of  $V^{51}$  in the amorphous phase is attributable primarily to the inhomogeneous Knight shift broadening. Consequently this behavior of the line broadening appears to confirm a long range oscillatory behavior of electron density in the amorphous phase of VZr alloy film.

The significant decrease in the line intensity of the amorphous phase relative to that of the crystalline phase appears to be consistent with Kohn-Vosko theory. It is suggested that quadrupole interaction of  $V^{51}$  with a large electric field gradient produced by the

lattice distortion and redistribution of the occupied electronic states is probably due to the gas impurities trapped in VZr alloy film. In order to make a definite conclusion about the long range charge density oscillations predicted by Friedel around the impurity, and quadrupole interaction with the electric field gradient in the amorphous transition metal alloy, NMR experiments with a series of the amorphous transition metal alloys that are free from gas impurities should be repeated. Amorphous metal films that are free from gas impurities can be prepared by electron beam evaporation of an alloy slug. Amorphous VTi and VCr systems would be suitable choices for NMR, magnetic susceptibility, and specific heat experiments in order to obtain the variation of 'd' and orbital contributions in these systems, and to study the long range oscillations and the quadrupole effects. NMR data for the VTi and VCr systems in the crystalline phase already exist for the purpose of comparison, and the NMR signal of  $V^{51}$  is strong compared with that of other transition metal elements.

## V. Acknowledgements

The author wishes to express his appreciation to the following persons:

Dr. Harlan E. Schone, his advisor, for his continued guidance and encouragement during the course of the experiment and in the preparation of the manuscript.

Drs. Jon F. Soest, Roy L. Champion, William J. Kossler and Melvyn D. Schiavelli for helpful discussions and careful reading of the manuscript.

Mr. Chris Gross, Glen Sachse and their staff, who are at NASA Langley Research Center, for the preparation and analysis of samples.

Mr. Stanley Hummel, Research Engineer, and his staff in the William and Mary Machine and Instrument Shop, for skillful construction of some of the equipment used in this research, and in particular, for the preparation of VZr target and substrates.

Miss Margaret Malone for her expert typing of the thesis on a very tight schedule.

His wife, Sook Ja, for her encouragement and understanding over the past six years.

## VI. References

1. E. A. Stern, Phys. Rev. 157, 544 (1967).
2. A. Blandin, E. Daniel, and J. Friedel, Phil. Mag. 4, 180 (1959).
3. A. Clogston, V. Jaccarino, Phys. Rev. 121, 1357 (1961).
4. W. D. Knight, Advances in Solid State Physics (Academic Press, Inc., New York, 1955) Vol. 2, pp. 93-136.
5. L. E. Drain, Proc. Phys. Soc., 83, 755 (1964).
6. J. Butterworth, Proc. Phys. Soc., 83, 71 (1964).
7. A. Narath, A. Fromhold, Phys. Rev., 139A, 794 (1964).
8. A. Clogston, A. Gossard, V. Jaccarino, Y. Yaft, Phys. Rev., 36, 170 (1964).
9. F. J. Blatt, Phys. Rev., 108, 285 (1957).
10. J. M. Ziman, Advance in Physics, 16, 421 (1967).
11. R. L. Odle, C. P. Flynn, Phil. Mag., 13, (1966).
12. E. C. Snow, J. T. Waber, ACTA META., 17, (1969).
13. L. F. Mattheiss, Phys. Rev., 134, 4A (1964).
14. D. O. Van Ostanburg, D. J. Lam, M. Shimizu, A. J. Katsuki, J. Phys. Soc. Japan, 18, 1744 (1963).
15. Y. Matsuda, M. Nishioka, J. Watanabe, J. Phys. Soc. Japan, 22, 238 (1967).
16. J. C. Swartz, L. J. Swartzendruber, R. E. Watson, Phys. Rev., B 1, 146 (1970).

17. L. H. Bennett, L. J. Swartzendruber, R. E. Watson, *Phys. Rev.*, 165, 500 (1968).
18. N. Bloemergen, T. J. Rowland, *ACTA, Met.*, 731 (1953).
19. W. Kohn, S. H. Vosko, *Phys. Rev.*, 119, 912 (1960).
20. T. J. Rowland, *Phys. Rev.*, 119, 900 (1960).
21. E. von Meerwall, T. J. Rowland, *Phys. Rev.*, B5, 2480 (1972).
22. M. M. Collver and R. H. Hammond, *Phys. Rev. Letters*, 30, 92 (1973).
23. J. Bardeen, L. N. Cooper, J. R. Schrieffer, *Phys. Rev.*, 108, 1175 (1957).
24. J. J. Hopfield, *Phys. Rev.*, 186, 443 (1969).
25. W. L. McMillan, *Phys. Rev.*, 167, 331 (1968).
26. J. W. Garland, K. H. Benneman, *Superconductivity in d- and f-Band Metals*, AIP Conference Proceedings No. 4 255 (1972).
27. J. E. Crow, M. Strongin, R. S. Thompson, O. F. Kammerer, *Phys. Letter*, 30A, 161 (1969).
28. M. M. Collver, Ph.D. Thesis, University of California, 97 (1971).
29. E. C. Snow, J. T. Waber, *ACTA. Met.*, 17, 623 (1969).
30. Cullity, Element of X-ray Diffraction (Addison-Wiley Co., Mass. 1968) pp. 262.
31. M. A. Niclet, J. W. Mayer, I. V. Mitchell, *Science* 177, 841 (1972).
32. F. N. H. Robinson, *J. Sci. Inst.*, 36, 1959.
33. M. Petrinovic, Rudjer Baskovic, Zagreb, Yugoslavia, unpublished.
34. D. H. Howling, *Rev. Sci. Instr.*, 37, 891 (1966).
35. G. D. Watkins, Ph.D. Thesis, Harvard University (1952).

36. R. P. Elliot, *The Constitution of Binary Alloys, First Supplement* (McGraw-Hill Book Company, New York, 1965), pp. 1253.
37. H. F. Winters, E. Kay, *J. Applied Phy.*, 38, 3928 (1967).
38. N. Waterhouse, P. S. Wilcox, D. J. Willmott, *J. Applied Phys.*, 42, 5649 (1971).
39. J. H. Van Vleck, *Phys. Rev.*, 74, 1168 (1948).
40. K. Kambe, J. F. Ollom, *J. Phys. Soc. Japan*, 11, 50 (1956).
41. M. A. Ruderman, C. Kittel, *Phys. Rev.* 96, 99 (1954).
42. N. Bloembergen, T. J. Rowland, *Phys. Rev.* 97, 1679 (1955).
43. Y. Masuda, M. Nishioka, *J. Phys. Soc. Japan*, 22, 238 (1967).
44. D. S. Schreiber, L. D. Graham, *J. Chem. Phys.* 42, 2573 (1965).
45. L. E. Drain, *Proc. Phys. Soc.*, 80, 1380 (1962).
46. R. E. Watson, L. H. Bennett, A. J. Freeman, *Phys. Rev.* 179, 590 (1969).

## VII. List of Tables

Table I Composition Analysis Data of VZr films.

Table II Knight Shifts and Linewidths of VZr films.

Table III Relative Line Intensity of VZr film between the  
Amorphous State and the Crystalline State (Annealed One).

## VIII. List of Figures

### Figure

1. Schematic Illustration of Conduction Electron Charge Screening Induced in a Metal Host by a Single Impurity.
2. Variation of Knight Shift with  $e/a$  ratio for Transition Metals of the 3d and 4d Rows.
3. Variation of Susceptibility and Density of States as Measured by Electronic Specific Heat, with  $e/a$  ratio for b.c.c. Transition Metals of 3d and 4d Rows.
4. Superconducting Transition Temperature of the As-deposited Vapor Quenched 4d Transition Metal Films Versus the Number of Electron per Atom.
5. Schematic Diagram of the Sputtering Module.
6. Block Diagram of NMR System.
7. Robinson Oscillator and Limiter Circuit.
8. Detector and Audio Sections for Robinson Oscillator Circuit.
9. Illustration of the Manner in Which the Derivative of the NMR Absorption Lines is Obtained by the Use of Field Modulation Small Compared to Linewidth.
10.  $\Delta K/K_V$  Versus Zr Concentration, VZr Alloy.
11.  $\Delta K/K_V$  Versus Field H, VZr Alloy (Amorphous phase).

## Figure

12.  $\Delta K/K_v$  Versus Field H, VZr Alloy (Crystalline phase).
13. Linewidth of  $V^{51}$  Versus Zr Concentration, VZr Alloy.
14. Linewidth of  $V^{51}$  Versus Field H, VAr<sup>17.2</sup> Alloy.
15. Linewidth of  $V^{51}$  Versus Field H, VZr<sup>28</sup> Alloy.
16. Linewidth of  $V^{51}$  Versus Field H, VZr<sup>46.4</sup> Alloy.